Simultaneous cooling and trapping of ^{6}Li and $^{85/87}$Rb

by

Janelle Van Dongen

A THESIS SUBMITTED IN PARTIAL FULFILMENT OF
THE REQUIREMENTS FOR THE DEGREE OF

Master of Science

in

The Faculty of Graduate Studies

(Physics)

The University Of British Columbia

December, 2007

Abstract

This thesis provides a summary of the laser system constructed in the Quantum Degenerate Gases Laboratory for laser cooling and trapping of $^{85/87}$Rb and ^{6}Li as well as of experiments that have been pursued in our lab to date. The first chapter provides an overview of the experimental focus of the QDG lab. The second and third chapters provide the fundamental theory behind laser cooling and trapping. The fourth chapter provides details of the laser system. The fifth chapter describes an experiment performed on the subject of dual-injection, performed in collaboration with Dr. James Booth of the British Columbia Institute of Technology (BCIT) involving the dual-injection of a single slave amplifier. The last chapter describes the progress made on the experimental setup needed for the study of Feshbach resonances between $^{85/87}$Rb and ^{6}Li and the photoassociative formation of molecules.

Table of Contents

List of Tables

List of Figures

Acknowledgements

Thank you to Dr. Kirk Madison for allowing me to work in the QDG lab and to stay on as a graduate student and nuisance in general. Thank you also for being an extremely talented, personable, and understanding supervisor, as well as a gifted teacher. I am very grateful for the help given so many times. Thank you also to Dr. Bruce Klappauf for his hard work, for lending his talent and proficiency to every aspect of the lab, for letting me empty his entire library and for helping on countless occasions. Thank you to Dr. Jim Booth for his good humour, collaboration, and valuable contributions, as well as for setting a precedent of firsts in our lab. There are several students with whom I have had the privilege of working with directly and would like to express gratitude to: Tao for his diverse abilities and being a foundational member, Swati for being a beam of sunlight in our lab, Keith for being patient and helping me on many occasions, Nina for being a fun and intelligent person, Bastian for his dedication to detail and being a pleasure to work with, and both Paul and Ray for the talent displayed in everything you guys are involved with.

Thank you to Dr. Mona Berciu for still answering her door when I knock after being asked for help over and over again and being extremely kind. Thank you also to Dr. Ovidiu Toader for bringing immense talent to the lab.

Thank you also to: Sylvain for his presence and important contribution to the Feshbach and Master table, Pavle for going the extra mile with the laser you and your classmates built, Aviv and Peter for their contributions and Jordan and Amy for being wonderful labmates.

Thanks to Dr. David Jones, Dr. Art Mills and Yifei for their involvement with the photoassociation/Feshbach experiment and the expertise they bring to this endeavour. Thanks also to T.J., Dr.Jie Jiang, Sybil and Rob for being nice people to be around.

Thank you to my Dad for the support and care.

Statement of Co-Authorship

The chapter on the miniature atom trap table- Dual injection study is based on a paper we recently published. My contributions to this study involved data collection and experimental setup. My contribution to the manuscript itself included writing a preliminary draft of the experimental section, work on the figures and final editing.

Chapter 1

Introduction

The purpose of this chapter is as a motivation for the experiments discussed in this thesis, with some theoretical background given to understand the rationale of the experiments being undertaken.

1.1 Quantum degenerate gases in optical lattices

The Hubbard model describing strongly correlated electron systems such as high-Tc superconductors (Tc meaning the ‘ critical temperature’ at which the electrical resisitance is zero) is of great fundamental importance to condensed matter theory. Providing experimental data which reveals its behaviour at low temperature would constitute a major scientific accomplishment. Placing a quantum degenerate Fermi gas into a three-dimensional periodic potential formed by the interference of light (known as an optical lattice, analagous to a crystal lattice) has been proposed as a possible means of studying this model [KMS$^+$05, HJICDL02, WPGH05]. This approach offers the advantages of precise control of the model parameters and elimination of impurities or defects.

1.1.1 The Hubbard model

The essence of the Hubbard model can be explained, following Ref. [Tas98], as a tight binding model of electrons with short-range Coulomb interactions. The electrons are located at the lattice sites and can hop (tunnel) between sites. For simplicity we will assume hopping (tunneling) only occurs between adjacent lattice sites. The hamiltonian describing this system can be written as

$$H = H_{hop} + H_{int} \tag{1.1}$$

where H_{hop} describes the hopping (tunneling) of the electrons between lattice sites and H_{int} represents the energy due to on site interactions

$$H_{hop} = \sum_{i,j} \sum_{\sigma=\uparrow,\downarrow} t_{i,j} c^{\dagger}_{i\sigma} c_{j\sigma} \tag{1.2}$$

i and j represent all possible lattice sites and σ represents the spin configuration of the electrons. $t_{i,j}$ represents the probability amplitude of an electron hopping from lattice site i to lattice site j. $c^{\dagger}_{i\sigma}$ and $c_{j\sigma}$, are fermion operators which create or annhilate an electron at lattice site i and j respectively with spin σ. The number operator which represents the number of electrons at lattice site i with spin σ is

$$n_{i,\sigma} = c^{\dagger}_{i\sigma} c_{i\sigma} \tag{1.3}$$

and has eigenvalues of 0 or 1 in accordance with the Pauli-exclusion principle.

The energy due to interactions between electrons occupying the same lattice site is described as

$$H_{int} = U \sum_{i} n_{i,\uparrow} n_{i,\downarrow} \tag{1.4}$$

where U is the energy associated with the repulsive interaction between two electrons at the same site.

1.1.2 QDG experimental approach

Our lab hopes to study aspects of the Hubbard model via ultracold atoms placed in optical lattices. In particular, we are interested in an insulating state where $U >> t$, where we call $t_{i,j} = t$ for all lattice sites, such that the electron hopping is suppressed and we are interested in achieving an antiferromagnetic state where the spins of the electrons are opposite at adjacent lattice sites. Electrons are fermions and we plan to use ^{6}Li (also fermions) as electron analogs. The troughs in light intensity of the standing wave used for the optical lattice serve as the lattice sites. U can be tuned by changing the intensity of the light, with the atoms becoming increasingly localized and interacting more strongly as the intensity is increased. Above the Néel temperature antiferromagnetic material becomes paramagnetic. For the case of large U/t the Néel temperature $T_N \propto \frac{t^2}{k_B U}$ [WPGH05].

The hopping/tunneling matrix elements and interaction energy can be expressed as [HJICDL02]

$$t = E_R \frac{2}{\sqrt{\pi}} \xi^3 \exp\left(-2\xi^2\right) \tag{1.5}$$

and

$$U = E_R a_s k \sqrt{\frac{8}{\pi}} \xi^3 \tag{1.6}$$

where $E_R = \hbar^2 k^2 / 2m$ is the atomic recoil energy, a_s is the scattering length, k is the light wavevector magnitude, and $\xi = (V_0/E_R)^{1/4}$ for lattice sites with potential depth V_0.

Currently, attempts to study the low temperature phases of the fermionic Hubbard model using either ^{6}Li or ^{40}K in optical lattices have been severely limited by the temperatures experimentally realizable. As an example, when $U/t \approx 10$ $T_N < 0.015 E_R$ (for ^{6}Li this is 5.6 μK). Special cooling schemes are required to attain the temperatures needed [WPGH05]. The preliminary phase of experiments being pursued by our lab aims to develop methods of reaching the temperatures needed while maintaining the condition that $U >> t$.

Feshbach resonances

Our lab hopes to develop a novel cooling technique to produce samples of ^{6}Li at temperatures lower than presently achievable and apply this to the study of ^{6}Li in an optical lattice. The cooling mechanism proposed is the use of Feshbach resonances to sympathetically cool ^{6}Li via elastic collisions with ^{85}Rb or ^{87}Rb, which are bosons and can be cooled to lower temperatures than ^{6}Li.

Feshbach resonances occur when an external magnetic field is tuned so that the collision energy of an unbound pair of atoms is degenerate with that of a molecular bound state of different spin configuration. At the resonance the collisional cross-section diverges and, therefore, by varying the magnetic field applied the collisional interactions between atoms can be tuned continuously [KGJ06]. The study of Feshbach resonances can be applied to controlling the interaction energy U, and to achieve colder atomic temperatures.

Photoassociation

Photoassociation refers to the process where two colliding atoms absorb a photon taking them to an excited molecular bound state [JTLJ06]. One experimental interest of the QDG laboratory is studying the formation of LiRb molecules in their rovibronic ground state. Placing LiRb molecules in an optical lattice provides a means of studying a many-body system with electric dipole-dipole interactions.

Preliminary investigation of Feshbach resonances and photoassociation for ^{6}Li and $^{85/87}$Rb are the lab's immediate experimental goals being undertaken in a collaborative effort with Prof. David Jones whose lab is across from ours.

1.2 Miniature atom trap experiment

The QDG lab also collaborates with Dr. James Booth of the British Columbia Institute of Technology on providing a more portable system for creating magneto-optical traps, making this physics more accessible for educational purposes. To this end investigations have been undertaken towards simplification of the optical apparatus, reduction of the vacuum equipment needed and compactness of the atom cell.

1.3 This Thesis

A precursor to all the experiments being mentioned above is the formation of ultracold samples of ^{6}Li, ^{85}Rb and ^{87}Rb. The creation of samples of ultracold atoms and molecules requires an immense infrastructure of optical, electronic and computer control systems. My contribution to this has been involvement in the construction of a system to provide frequency stabilized laser light ($\frac{\Delta f}{f} \sim 2 \times 10^{8}$) at sufficient powers to be used for a dual species magneto-optical trap (MOT) to initially cool and trap $^{85/87}$Rb and ^{6}Li.

The beginning chapters (2 and 3) of this thesis provide a background knowledge of laser cooling and trapping and applications pertinent to the experimental setup of the QDG laboratory such as magneto-optical traps and optical dipole traps. Chapter 4 describes the 'master table' which is the starting point for generation of light needed for the cooling and trapping of our atomic samples. Chapter 5 describes an experimental study of the dual injection of a slave amplifier performed to further the Miniature Atom Trap experiment. Chapter 6 provides information on the developments of the experimental study on the photoassociative creation of LiRb molecules as well as preliminary investigations of Feshbach resonances between ^{6}Li and $^{85/87}$Rb.

Chapter 2

Light-Matter interaction

This chapter provides an introduction to the concepts of radiation pressure and dipole force which are the fundamental mechanisms involved in laser cooling and trapping.

A foundational concept of light-matter interaction is that the electric field part, $\mathbf{E}$, of the the electro-magnetic wave induces a dipole moment $\mathbf{d} = -e\mathbf{r}$ on a neutral atom. $\mathbf{r}$ is the coordinate of the electron with respect to the nucleus (for a multi-electron atom it is the sum of the coordinates of the individual electrons)and is typically small (a few angstroms) compared with the wavelength of optical radiation (thousands of angstroms). The energy of this induced dipole can be taken in the dipole approximation to be $-\mathbf{d}\cdot\mathbf{E}$ [ME88, Gri89]. We focus on the effect of the electric field because it is significantly larger than the effect of the magnetic field for non-relativistic particle speeds [ME88].

2.1 Forces due to light-matter interaction

Expanding our interest from the interaction of light with one atom to many, we introduce the concept of polarization as the dipole moment per unit volume.

$$\mathbf{P} = \frac{\mathbf{d}}{V} \tag{2.1}$$

In a linear dielectric medium we can also express the polarization as

$$\mathbf{P} = \epsilon_0 \chi \mathbf{E} \tag{2.2}$$

where χ is the electric susceptibility. In general, χ is a tensor but for an isotropic medium it can be expressed as a scalar.

2.1.1 Electron oscillator model

In the classical electron oscillator model the electron is treated as if attached to the nucleus by a spring with the dipole moment oscillating as the field oscillates. Introducing frictional damping into this model results in a phase shift of the oscillation of the dipole moment with respect to the field [ME88]. This can be taken into account by treating the susceptibility as a complex quantity

$$\chi(\omega) = \chi'(\omega) + i\chi''(\omega) \tag{2.3}$$

giving

$$\mathbf{P} = \epsilon_0(\chi' + i\chi'')\mathbf{E} = \mathbf{P}_{dis} + \mathbf{P}_{abs} \tag{2.4}$$

The real part of the susceptibility is in phase with the field and is associated with dispersion whereas the imaginary part is associated with absorption. χ'' is proportional to the absorption cross section, σ [WH03]. The polarization can then also be expressed as a real dispersive part, $\mathbf{P}_{dis}$, and an imaginary absorptive part, $\mathbf{P}_{abs}$.

For the case where the field is a plane wave travelling in the positive z direction we can write the polarization as

$$\mathbf{P} = \epsilon_0(\chi' + i\chi'')\mathbf{E_0}e^{i(kz-\omega t)} \tag{2.5}$$

2.1.2 Derivation of light forces

The following derivation for the forces light exerts on atoms provides a summary of a more detailed description found in Ref.[WH03].

The force density on the atoms due to the light-matter interaction can be expressed as

$$\mathbf{F} = Re[-\nabla(-\mathbf{P} \cdot \mathbf{E}^*)] \tag{2.6}$$

Substituting Eq. 2.5 into the above equation and averaging over an optical cycle we have

$$\langle \mathbf{F} \rangle = \frac{1}{4}\epsilon_0\chi'\nabla E_0^2 + \frac{1}{2}\epsilon_0\chi'' E_0^2 k\mathbf{z} \tag{2.7}$$

The first term of this equation represents a force that directs the atoms along the gradient of intensity and is called the *dipole-gradient force* or *dipole force*, the second term represents a force acting along the direction of light propagation and is called the *radiation pressure force* arising from absorption and spontaneous emission of light by the atom. For a travelling wave the dipole force is neglible compared to the radiation pressure but for cases where a large gradient in the field exists (an example being a highly focused beam or a standing wave) this force can be strong enough to trap the atoms and is applied for this purpose in optical dipole traps. The radiation pressure can be applied to slow down atoms and forms the basis of laser cooling.

It is useful to write these forces in more detail considering two levels atoms in state ψ written in a basis of energy eigenstates ($E_1 = \hbar\omega_1$, $E_2 = \hbar\omega_2$),

$$\psi = c_1\psi_1(\mathbf{r})e^{-i\omega_1 t} + c_2\psi_2(\mathbf{r})e^{-i\omega_2 t} \tag{2.8}$$

The polarization being the dipole moment density can be written as

$$\begin{aligned} P &= \frac{N}{V}\langle\psi|\mathbf{d}|\psi\rangle \\ &= \frac{N}{V}[c_1^* c_2 \mathbf{d}_{12} e^{-i\omega_0 t} + c_2^* c_1 \mathbf{d}_{21} e^{i\omega_0 t}] \\ &= \frac{N}{V}\mathbf{d}_{12}[c_1^* c_2 e^{-i\omega_0 t} + c_2^* c_1 e^{i\omega_0 t}] \end{aligned} \tag{2.9}$$

with $\omega_0 = \omega_2 - \omega_1$, $\mathbf{d}_{12} = \langle\psi_1|\mathbf{d}|\psi_2\rangle$, $\mathbf{d}_{21} = \langle\psi_2|\mathbf{d}|\psi_1\rangle$ and using $\mathbf{d}_{12} = \mathbf{d}_{21}$ and $\langle\psi_1|\mathbf{d}|\psi_1\rangle = \langle\psi_2|\mathbf{d}|\psi_2\rangle = 0$.

Solving for the steady state optical bloch equations and including the spontaneous emission rate, Γ, gives [WH03]

$$c_1 c_2^* = e^{i\Delta t}\frac{\frac{1}{2}\Omega_0(\Delta - i\frac{\Gamma}{2})}{\Delta^2 + (\frac{\Gamma}{2})^2 + \frac{1}{2}|\Omega_0|^2} \tag{2.10}$$

with

$$\Gamma = \frac{\omega_0^3|\mathbf{d}_{12}|^2}{3\pi\epsilon_0\hbar c^3} \tag{2.11}$$

where $\Delta = \omega - \omega_0$ and

$$\Omega_0 = -\frac{\mathbf{d}_{12}\cdot\mathbf{E}_0}{\hbar} \tag{2.12}$$

for the travelling wave which we are considering. This expression for $c_1c_2^\star$ can be substituted into Eq. 2.10 for the polarization which in comparison to the form of the polarization given in Eq. 2.5 provides an expression for the electric susceptibility as

$$\chi = \frac{N\mathbf{d}_{12}^2}{3\epsilon_0\hbar V}\left(-\frac{\Delta}{\Delta^2 + (\Gamma/2)^2 + \frac{1}{2}|\Omega_0|^2} + i\frac{\Gamma/2}{\Delta^2 + (\Gamma/2)^2 + \frac{1}{2}|\Omega_0|^2}\right) \tag{2.13}$$

Finally we can write the expressions for the dipole gradient force,$\mathbf{F}_{dip}$ and the radiation pressure,$\mathbf{F}_{rad}$ due to a travelling wave acting on a collection of two level atoms given in Eq. 2.7 as:

$$\mathbf{F}_{dip} = \frac{1}{4}\epsilon_0\nabla E_0^2\left[\frac{\mathbf{d}_{12}^2}{3\epsilon_0\hbar}\left(-\frac{\Delta}{\Delta^2 + (\Gamma/2)^2 + \frac{1}{2}|\Omega_0|^2}\right)\right] \tag{2.14}$$

$$\mathbf{F}_{rad} = \frac{1}{2}\epsilon_0 E_0^2 k\mathbf{z}\left[\frac{\mathbf{d}_{12}^2}{3\epsilon_0\hbar}\left(\frac{\Gamma/2}{\Delta^2 + (\Gamma/2)^2 + \frac{1}{2}|\Omega_0|^2}\right)\right] \tag{2.15}$$

Comparing the dipole gradient force to the radiation pressure we see that the direction of the dipole force changes depending on whether the detuning Δ is positive or negative. For a negative detuning the atom is attracted to regions of highest intensity whereas for positve detuning the atom is repelled. By contrast, the radiation pressure, does not depend on the sign of the detuning. Also the radiation pressure has a $1/\Delta^2$ dependence whereas the dipole force has a $1/\Delta$ dependence so that for small detunings where the light frequency is close to the atomic resonance the radiation pressure dominates but when the detuning is large the dipole force dominates. The next section will explore the dipole force in the 'dressed atom approach' both to develop further knowledge necessary to understand the intricacies of laser cooling and trapping and for exposure to quantum mechanical theory of light-matter interaction.

2.2 Dressed Atom approach

In the discussion of light matter interaction up to this point we have adopted a semi-classical view where the light is a classical wave and the atom energy is quantized having discrete levels. It is useful to consider a full quantum treatment of the dressed atom formalism. Later the semi-classical picture will be revisited, incorporatign the dressed atom scheme.

2.2.1 Quantum Dressed Atom approach

Hamiltonian

The full Hamiltonian, H, for an atom interacting with a light field of frequency ω is given as [CTDRG92]

$$H = H_a + H_f + H_{int} \tag{2.16}$$

H_a is the hamiltonian for the atom. It can be expressed as

$$\sum_i E_i |i\rangle\langle i| \tag{2.17}$$

with i labelling the different energy eigenstates with energy E_i. H_f is the hamiltonian for the light field with

$$H_f = \hbar\omega(a^\dagger a + 1/2) \tag{2.18}$$

where the eigenstates of H_f are the photon number states $|n\rangle$ with $n = 0, 1, 2\ldots$ representing the number of photons in the light field at frequency

ω. The photon creation and anhilation operators, $a^\dagger$ and a, respectively, act such that

$$a|n\rangle = \sqrt{n}|n-1\rangle \tag{2.19}$$

$$a^\dagger|n\rangle = \sqrt{(n+1)}|n+1\rangle. \tag{2.20}$$

The energy associated with $|n\rangle$ is

$$E_n = (n+1/2)\hbar\omega. \tag{2.21}$$

H_{int} accounts for the interaction between the atom and light field. In the dipole approximation H_{int} is given by

$$H_{int} = -\mathbf{d}\cdot\mathbf{E} \tag{2.22}$$

where $\mathbf{d}$ is the dipole moment operator and $\mathbf{E}$ the electric field operator. This form of the interaction term can be understood as in the semiclassical picture in the last section as the field inducing a dipole moment on the atom.

To find the energies associated with the full hamiltonian H of the atom and the field we express H in terms of the product basis of the atomic eigenstates and the photon number states which are eigenstates of $H_a + H_f$. If we assume, for simplicity, that the atom has only two energy levels with eigenstates $|1\rangle$ for the ground state and $|2\rangle$ for the excited state, this product basis consists of $|1\rangle \otimes |n\rangle \equiv |1,n\rangle$ and $|2\rangle \otimes |n\rangle \equiv |2,n\rangle$ with $n = 0, 1, 2 \ldots$. The product basis is referred to as the *bare states* and the *dressed states* are eigenvectors of the hamiltonian. The dressed atom approach involves diagonalizing the hamiltonian in the bare state basis and finding the eigenvectors and eigenenergies corresponding to the dressed states [Dra96].

$\mathbf{H}_{int}$ revisited

The dipole moment operator is expressed as [WH03]

$$\begin{aligned}\mathbf{d} &= \sum_{i=1,2} |i\rangle\langle i|\mathbf{d} \sum_{j=1,2} |j\rangle\langle j| \qquad (2.23)\\ &= \sum_{i,j} \langle i|\mathbf{d}|i\rangle |i\rangle\langle j|\end{aligned}$$

where $\langle i|\mathbf{d}|j\rangle = \mathbf{d}_{ij}$ are the dipole matrix elements, which have the properties that $\mathbf{d}_{12} = \mathbf{d}_{21}$ and $\mathbf{d}_{11} = \mathbf{d}_{22} = 0$ [WH03]. This gives

$$\mathbf{d} = \mathbf{d}_{12}(|1\rangle\langle 2| + |2\rangle\langle 1|) \tag{2.24}$$

with $|1\rangle\langle 2|$ and $|2\rangle\langle 1|$ being respectively the atomic state lowering and raising operators. The vector quality of the dipole operator is contained in the dipole matrix element.

The electric field operator, $\mathbf{E}$ for a single mode, $\mathbf{k}$ of the field constrained by a volume V can be expressed in terms of the photon creation and anhilation operators as

$$\mathbf{E} = \sqrt{\frac{\hbar\omega}{2\epsilon_0 V}}\hat{\epsilon}\left(ae^{i\mathbf{k}\cdot\mathbf{r}-\omega t} + a^\dagger e^{-i\mathbf{k}\cdot\mathbf{r}-\omega t}\right) \tag{2.25}$$

where $\hat{\epsilon}$ is the polarization vector of the field [WH03, CTDRG92]. When evaluating $-\mathbf{d}\cdot\mathbf{E}$ terms involving products of the photon creation and state raising operators ($a^\dagger$ and $|2\rangle\langle 1|$) or the photon anhilation and state lowering operators (a and $|1\rangle\langle 2|$) are ignored in the rotating wave approximation where the detuning of the light freqeuncy from the atomic transition frequency is much less than the light frequency, $\Delta = \omega - \omega_0 << \omega$. These terms are important, however, for higher order processes such as multiphoton absorption or Raman scattering processes [Dra96, WH03]. In the rotating wave appoximation then we have an interaction term of

$$\begin{aligned} H_{int} &= -\sqrt{\frac{\hbar\omega}{2\epsilon_0 V}}\mathbf{d}_{12}\cdot\hat{\epsilon}\left(|2\rangle\langle 1|ae^{i(\mathbf{k}\cdot\mathbf{r}-\omega t)} + |1\rangle\langle 2|a^\dagger e^{-i(\mathbf{k}\cdot\mathbf{r}-\omega t)}\right) \\ &= g\left(|2\rangle\langle 1|ae^{i(\mathbf{k}\cdot\mathbf{r}-\omega t)} + |1\rangle\langle 2|a^\dagger e^{-i(\mathbf{k}\cdot\mathbf{r}-\omega t)}\right) \end{aligned} \tag{2.26}$$

where [CTDRG92]

$$g = -\sqrt{\frac{\hbar\omega}{2\epsilon_0 V}}\mathbf{d}_{12}\cdot\hat{\epsilon} \tag{2.27}$$

Dressed states and eigenenergies

Both H_a and H_f only contain diagonal elements in the product basis. $H_{int} = -\mathbf{d}\cdot\mathbf{E}$, however, only couples off diagonal elements of the form $|1, n+1\rangle$ and $|2, n\rangle$ (ignoring higher order processes) so that with the appropriate ordering of product basis states the full hamiltonian, H, is an infinite block diagonal matrix with two by two matrices along the diagonal. These two by two matrices will have the form

$$\begin{pmatrix} \langle 1, n+1|H|1, n+1\rangle & \langle 1, n+1|H|2, n\rangle \\ \langle 2, n|H|1, n+1\rangle & \langle 2, n|H|2, n\rangle \end{pmatrix} \tag{2.28}$$

$$= \begin{pmatrix} 0 & g\sqrt{n+1}e^{-i(\mathbf{k}\cdot\mathbf{r}-\omega t)} \\ g\sqrt{n+1}e^{i(\mathbf{k}\cdot\mathbf{r}-\omega t)} & -\hbar\Delta \end{pmatrix}$$

For convenience the product basis state $|1, n+1\rangle$ is taken to have an energy of zero.

The eigenvalues of 2.29 are

$$E_{\pm} = -\frac{\hbar\Delta}{2} \pm \frac{1}{2}\sqrt{(\hbar\Delta)^2 + 4g^2(n+1)} \tag{2.29}$$

The dressed states, $|\psi_{\pm}(n)\rangle$, corresponding to the energies $E\pm$ with n denoting a particular energy 'manifold' are given below [Dra96, CTDRG92]. A manifold is the set of enery levels E_+ and E_- for a particular choice of photon number, n, in the bare states.

$$|\psi_+(n)\rangle = \sin\theta|1, n+1\rangle + \cos\theta|2, n\rangle \tag{2.30}$$

$$|\psi_-(n))\rangle = \cos\theta|1, n+1\rangle - \sin\theta|2, n\rangle \tag{2.31}$$

with the Stückelberg angle, θ given by

$$\tan 2\theta = -2g\sqrt{n+1}/\Delta \tag{2.32}$$

$$0 \leq 2\theta \leq \pi$$

Light Shifts

Fig.2.1 shows how the energy of the $|2, n\rangle$ bare state is separated from the energy of the state $|1, n+1\rangle$ by $-\hbar\Delta$, with $|2, n\rangle$ being higher in energy for red detuning ($\Delta < 0$) and lower in energy for blue detuning ($\Delta > 0$). When comparing the energies of the dressed states with those of the bare states, we see that for an atom in its atomic ground state $|1, n\rangle$ the interaction of the light with the atom causes the state to have a lower energy when $\Delta < 0$ and a higher energy when $\Delta > 0$ with the opposite being the case for the $|2, n\rangle$ state. The difference between a bare state energy and its associated dressed state energy is called a *light shift* or an *AC Stark shift* and by Eq. 2.29 we have shifts of $\Delta_{\pm} = \pm(\frac{\hbar\Delta}{2} + \beta)$, where we let $\beta = \sqrt{(\hbar\Delta)^2 + 4g^2(n+1)}$ for convenience.

2.2.2 Semi-Classical Dressed State Approach

While useful to introduce the concepts of absorption and emission in terms of a change in the total number of photons in the light field, the semi-classical approach sufficiently describes the aspects of light-matter interaction for single mode light described by a coherent state [CTDRG92].

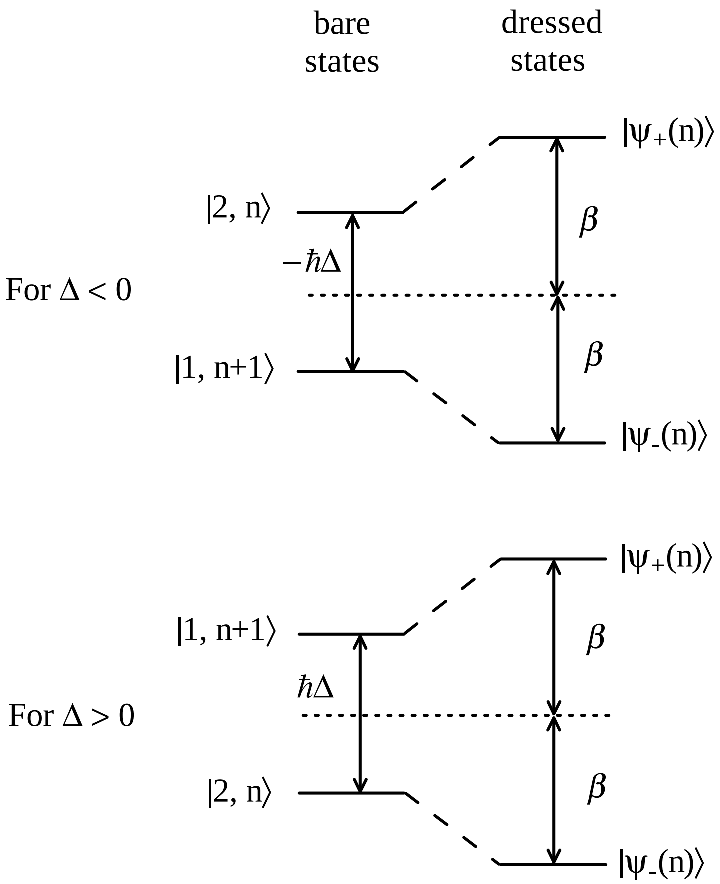

Figure 2.1: Relative energy of the $|1, n+1\rangle$ and $|2, n\rangle$ bare states for $\Delta < 0$ and $\Delta > 0$. In the presence of light the lower energy bare state is shifted down and the higher energy bare state is shifted up in energy giving an AC Stark shift of $\frac{\hbar\Delta}{2} + \beta$.

Hamiltonian

Without quantizing the electric field the hamiltonian for an atom including interaction with light is

$$H = H_A + H_{int} \tag{2.33}$$

where the atomic hamiltonian H_A is the same as before and $H_{int} = -\mathbf{d} \cdot \mathbf{E}$ but $\mathbf{E}$ is no longer an operator and is written

$$\mathbf{E} = \mathbf{E}^+ + \mathbf{E}^- \tag{2.34}$$

with $\mathbf{E}^\pm$ being the part of the field associated with $e^{\pm i\omega t}$ [Ste98b]. Note that $\mathbf{E}^+$ and $\mathbf{E}^-$ are complex conjugates of one another.

Form of H_{int}

The interaction term now takes the form

$$H_{int} = \mathbf{d}_{12} \cdot (\mathbf{E}^+ + \mathbf{E}^-)(|1\rangle\langle 2| + |2\rangle\langle 1|) \tag{2.35}$$

Again in the rotating wave approximation we neglect the product terms $E^+|1\rangle\langle 2|$ and $E^-|2\rangle\langle 1|$ giving

$$\begin{aligned} H_{int} &= \mathbf{d}_{12} \cdot \mathbf{E}^+|2\rangle\langle 1| + \mathbf{d}_{12} \cdot \mathbf{E}^-|1\rangle\langle 2| \\ &= \frac{\hbar\Omega}{2}|2\rangle\langle 1| + \frac{\hbar\Omega^*}{2}|1\rangle\langle 2| \end{aligned} \tag{2.36}$$

where the numerical factor

$$\frac{\hbar\Omega}{2} = \mathbf{d}_{12} \cdot \mathbf{E}^+ \tag{2.37}$$

Ω is called the *natural Rabi frequency* which we have briefly encountered already in section 1.

Dressed states and eigenenergies

At this point it is common to the rotating laser frame where the time dependence of $\mathbf{E}^\pm$ is removed and the excited atomic state $|2\rangle$ is replaced by $|2\rangle e^{i\omega t}$ with the ground state $|1\rangle$ remaining unchanged [Ste98b]. In this frame the separation of the atomic energy levels is $-\hbar\Delta$ so that the atomic hamiltonian can be expressed as

$$H_A = -\hbar\Delta|2\rangle\langle 2| \tag{2.38}$$

with the energy of the ground state taken to be zero.

The hamiltonian H can then be expressed as a two by two matrix in the atomic energy eigenstate basis giving

$$\begin{pmatrix} \langle 1|H|1\rangle & \langle 1|H|2\rangle \\ \langle 2|H|1\rangle & \langle 2|H|2\rangle \end{pmatrix} = \begin{pmatrix} 0 & \frac{\hbar\Omega}{2} \\ \frac{\hbar\Omega}{2} & -\hbar\Delta \end{pmatrix} \tag{2.39}$$

The eigenvalues of this hamiltonian are given as

$$E_{\pm} = -\frac{\hbar\Delta}{2} \pm \frac{\hbar\Omega'}{2} \tag{2.40}$$

where Ω' is the *generalized Rabi frequency*

$$\Omega' = \sqrt{\Delta^2 + \Omega^2} \tag{2.41}$$

The eigenfunctions (the dressed states) are [Dra96]

$$|\psi_+\rangle = \sin\theta|1\rangle + \cos\theta|2\rangle \tag{2.42}$$

$$|\psi_-\rangle = \cos\theta|1\rangle - \sin\theta|2\rangle \tag{2.43}$$

The Stückelberg angle θ is given by

$$\begin{gathered} \tan 2\theta = -\frac{\Omega}{\Delta} \\ 0 \leq 2\theta \leq \pi \end{gathered} \tag{2.44}$$

Light Shifts

The light shifts in the semiclassical dressed state for $\Delta < 0$ are given by

$$\Delta E_1 = -(\frac{\hbar\Omega'}{2} + \frac{\hbar\Delta}{2}) \tag{2.45}$$

$$\Delta E_2 = \frac{\hbar\Omega'}{2} + \frac{\hbar\Delta}{2} \tag{2.46}$$

for the ground and excited states respectively. For positive detuning the $|2\rangle$ state would be lower in energy than the $|1\rangle$ state.

In the limit where $\Omega << |\Delta|$ the light shifts become [Mv99]

$$\Delta E_1 = -\frac{\hbar\Omega^2}{4\Delta} \tag{2.47}$$

$$\Delta E_2 = \frac{\hbar\Omega^2}{4\Delta} \tag{2.48}$$

Expression for the dipole force

As an example that the dressed state approach where we solve for the eigenvalues and eigenvectors of the hamiltonian agrees with the semiclassical discussion above we will derive the identical expression for dipole force. The original derivation can be found in Ref. [CTDRG92]

A dressed atom in a $|\psi_+\rangle$ state will experience a force $F_+ = -\frac{\hbar}{2}\nabla\Omega'(\mathbf{r})$ and a force $F_- = -F_+$ for a $|\psi_-\rangle$ state. In a steady state situation the atom would experience a mean dipole force given by

$$\langle F_d\rangle = F_+P_+ + F_-P_- = -\frac{\hbar}{2}\nabla\Omega'(\mathbf{r})[P_+ - P_-] \tag{2.49}$$

where P_- and P_+ are the sum of the steady-state populations of each of the $|\psi_-\rangle$ and $|\psi_+\rangle$ states respectively. P_- and P_+ are given as

$$P_+ = \frac{\sin^4\theta}{\cos^4\theta + \sin^4\theta} \tag{2.50}$$

$$P_- = \frac{\cos^4\theta}{\cos^4\theta + \sin^4\theta} \tag{2.51}$$

with θ again being the Stückelberg angle referred to in Eq. 2.45. Substituting the expressions for P_- and P_+ given above and Eq. 2.41 for $\Omega'(\mathbf{r})$ into Eq. 2.49 we obtain the following expression for the mean dipole force:

$$\langle F_d\rangle = \frac{\hbar\Delta}{4}\frac{\nabla(\Omega^2)}{\Delta^2 + \frac{\Gamma^2}{4} + \frac{\Omega^2}{2}} \tag{2.52}$$

which is identical to the form we had previously derived.

2.3 Light shifts for multilevel atoms

For real atoms there exists hyperfine structure due to the coupling of the total electron angular momentum J and the total nuclear angular momentum I giving a total atomic angular momentum $F = I + J$. To find the light shift induced by the field on a particular hyperfine state $|F, m_F\rangle$ we will need to calculate the dipole matrix elements between hyperfine states. The beginning sections discuss this calculation and then we will discuss expressions for the light shift for two regimes of light frequency, where the light frequency is close to an atomic resonance involving $|F, m_F\rangle$ and where the light is far detuned.

2.3.1 Spherical basis

For convenience we will express the components of $\mathbf{d}_{12}$ and $\mathbf{E}$ in the spherical basis vectors [Ste98a, Zar88], $\hat{e}_{\pm 1}$, $\hat{e}_0$ where

$$\begin{aligned} \hat{e}_{\pm 1} &= \mp \frac{1}{\sqrt{2}}(\hat{x} \pm i\hat{y}) && (2.53) \\ \hat{e}_0 &= \hat{z} && (2.54) \end{aligned}$$

so that if $\mathbf{A} = A_x\hat{x} + A_y\hat{y} + A_z\hat{z}$ then

$$\begin{aligned} A_{\pm 1} &= \hat{e}_{\pm 1} \cdot \mathbf{A} = \mp \frac{1}{\sqrt{2}}(A_x \pm iA_y) && (2.55) \\ A_0 &= \hat{e}_0 \cdot \mathbf{A} = A_z && (2.56) \end{aligned}$$

In the spherical basis the dot product of two vectors is given as

$$\mathbf{A} \cdot \mathbf{B} = \sum_q (-1)^q A_q B_{-q} \tag{2.57}$$

$H_{int} = -\mathbf{d} \cdot \mathbf{E}$ in the spherical basis then is

$$\frac{\hbar\Omega}{2} = \sum_q (-1)^q \mathbf{d}_q E_{-q} \tag{2.58}$$

A useful part of expressing the vectors in the spherical basis is that if the polarization of the electric field is $\epsilon = \hat{e}_{\pm 1}$ this corresponds to left and right circularly polarized light respectively. $\epsilon = \hat{e}_0$ corresponds to linearly polarized light (polarized along the z axis). This means that for left and right circularly polarized light only $E_{\pm 1}$ are non zero respectively and for linear polarized light only E_0 is nonzero polarized along $\hat{z}$: if along $\hat{x}$ or $\hat{y}$ have combinations of E_{+1} and E_{-1}. This reduces the computation involved in solving for the dipole matrix element components described in the next section.

2.3.2 Dipole matrix elements

The dipole matrix elements take the form

$$\langle F, m_F|\mathbf{d}|F', m_{F'}\rangle_q = -e\langle F, m_F|\mathbf{r}|F', m_{F'}\rangle_q \tag{2.59}$$

with $q = \pm 1, 0$. Noting that

$$\begin{aligned} r_{\pm 1} &= \mp(x \pm iy) & (2.60)\\ r_0 &= z & (2.61) \end{aligned}$$

and that the spherical harmonics Y_{1q} can be expressed as

$$\begin{aligned} Y_{1q}(\theta, \phi) &= \frac{1}{r}\sqrt{\frac{3}{4\pi}}r_q & (2.62)\\ q &= \pm 0, 1 \end{aligned}$$

we have

$$\mathbf{r}\cdot\hat{e}_q = r_q = r\sqrt{\frac{4\pi}{3}}Y_{1q}(\theta, \phi) \tag{2.63}$$

so that the dipole matrix element components take the form

$$\langle F, m_F|\mathbf{d}|F', m_{F'}\rangle_q = -e\sqrt{\frac{4\pi}{3}}\langle F, m_F|rY_{1q}|F', m_{F'}\rangle \tag{2.64}$$

which can also be expressed using the Wigner-Eckart theorem [Ste01, Zar88] as

$$\langle F, m_F|\mathbf{d}|F', m_{F'}\rangle_q = -e\sqrt{\frac{4\pi}{3}}\langle F||r||F'\rangle\langle F, m_F|1, q|F', m_{F'}\rangle \tag{2.65}$$

$\langle F||r||F'\rangle$ is called a reduced matrix element and the second term is the standard Clebsch-Gordan coefficient.

Ref. [Ste01] shows how to solve for the reduced matrix element. In terms of a 3-j symbol we have

$$\langle F, m_F|\mathbf{d}|F', m_{F'}\rangle_q = -e\langle F||r||F'\rangle(-1)^{F'-1+m_F}\sqrt{2F+1}\begin{pmatrix} F' & 1 & F \\ m_{F'} & q & -m_F \end{pmatrix} \tag{2.66}$$

Using $F = J+I$ where J and I are the total electron and nuclear angular momentum, respectively, the reduced matrix element itself can be further expressed in terms of a 6-j symbols as

$$\langle F||r||F'\rangle = \langle J||r||J'\rangle(-1)^{F'+J+1+I}\sqrt{(2F'+1)(2J+1)}\left\{\begin{array}{ccc} J & J' & 1 \\ F' & F & I \end{array}\right\} \tag{2.67}$$

$\langle J||er||J'\rangle$ can be found from the lifetime of the transition from $|F', m_{F'}\rangle$ to $|F, m_F\rangle$, τ, using

$$\frac{1}{\tau} = \frac{\omega^3}{3\pi\epsilon_0\hbar c^3}\frac{2J+1}{2J'+1}|\langle J||er||J'\rangle|^2 \tag{2.68}$$

Note that when calculating $\langle F, m_F|\mathbf{d}|F', m_{F'}\rangle_q$ as described above, the Clebsch-Gordan coefficients are only non-vanishing when $m_{F'} = m_F - q$. This cancels the need for the sum over $m_{F'}$ and leads to the requirement that for right/left circularly polarized light $m_{F'} = m_F \pm 1$, and for linear polarized light $m_F = m_{F'}$. In other words for linear or circularly polarized light for each magnetic sublevel of a hyperfine state transitions are only allowed to one particular magnetic sublevel for each of the other hyperfine levels.

2.3.3 Expression for the light shift

Small detuning

For the case where the light frequency is close to an atomic frequency between ground state hyperfine level $|F, m_F\rangle$ and excited state $|F', m_{F'}\rangle$ then to find the light shift induced by the field we can extend previous discussion of light shifts for a two level atom.

The natural Rabi frequency expressed using the spherical basis is

$$\frac{\hbar\Omega}{2} = \sum_{m_{F'}}\sum_{q}(-1)^q\langle F, m_F|\mathbf{d}|F', m_{F'}\rangle_q E^+_{-q} \tag{2.69}$$

With further simplifications possible when q only takes on one of ±1 or 0 depending on the polarization of the light. Also the sum over $m_{F'}$ is redundant since as noted above $m_{F'} = m_F - q$.

The light shift can then be calculated in the same manner as in Eq. 2.43

Large detuning

For the case where the light is far detuned from atomic resonance then the approach to calculate the shift on a particular hyperfine level must incorporate the coupling between all other hyperfine levels. In this case lowest order perturbation theory gives the result that the shift on a ground state level, $|F, m_F\rangle$, denoted ΔE_g due to the excited states $|F', m_{F'}\rangle$, where $F' > F$, can be expressed as [TT95]

$$\Delta E_g = \frac{1}{4\hbar} \sum_e |\mathbf{d}_{eg} \cdot \mathbf{E}^+|^2 \left[\frac{1}{\omega_{eg} - \omega} + \frac{1}{\omega_{eg} + \omega} \right] \tag{2.70}$$

Here g and e represent the ground and excited states respectively and $\mathbf{d}_{eg} = \langle F', m_{F'} | \mathbf{d} | F, m_F \rangle$. Again there will be simplifications based on polarization choice.

Chapter 3

Laser Cooling and Trapping

3.1 Optical Molasses

Radiation pressure as we saw briefly in chapter 2 refers to the force on an atom due to absorption and spontaneous emission of light. Each time an absorption/emission event occurs the atom experiences a change in momentum $\hbar(\mathbf{k}-\mathbf{k}')$ where $\mathbf{k}$ is the wave vector of the absorbed photon and $\mathbf{k}$' that of the spontaneously emitted photon. Because the spontaneously emitted photons are emitted in random directions, the net force on the atom due to emission averages to zero and there is a force on the atom in the direction of propagation of the absorbed photons. Fig.3.1 shows a pictorial representation of this.

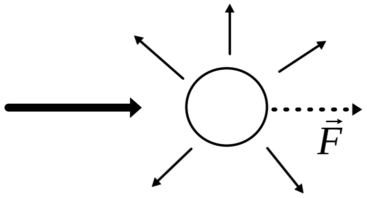

Figure 3.1: Light incident on the atom from the left travelling to the right exerts a force on the atom due to the momentum acquired by the atom from photon absorption. The emission of photons occurs in random directions with the force on the atom due to emission averaging to zero and the net force on the atom being in the directioin of light propagation.

If the light is detuned below a given atomic resonance such that when the atom is travelling toward the light it sees the frequency doppler shifted an atomic resonance then it will absorb from the light beam and experience slowing or cooling by the mechanism just described. Atoms going in the direction of the light propagation will see the light frequency further detuned from resonance and will not be affected. Shining red detuned light (light whose frequency is below an atomic frequency) on the atoms from all six directions creates a region at the intersection of the beams where atoms moving in all directions are slowed. The light in this region is called *optical molasses* [Mv99].

3.2 Magneto-Optical Trapping

3.2.1 Magnetic field

Though the atoms are slowed in optical molasses they are not spatially confined and can diffuse out of the intersection region. To provide spatial confinement a magnetic field is added along with appropriate choices of light polarization to create a magneto-optical trap (MOT). One possible realization is to have two magnetic coils placed in antiHelmholtz configuration creating a region of zero field at the center of the coils which increases linearly away from the center (see Fig.3.2).

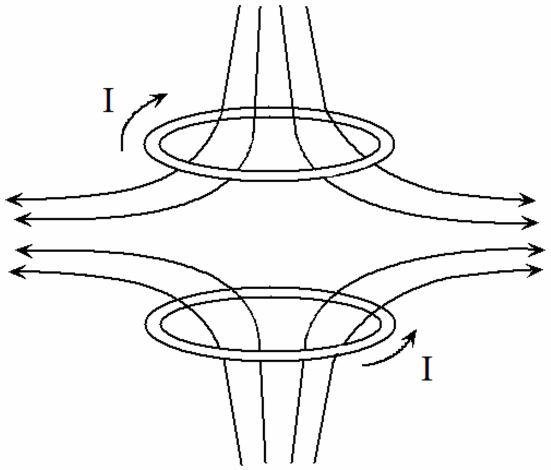

Figure 3.2: The magnetic field lines generated by passing current I through two coils in opposite directions for each coils (antiHelmholtz configuration). The magnetic field is the zero at the center between the coils and increasing in magnitude away from the center.

The MOT is formed by intersecting three pairs of mutually orthogonal circularly polarized laser beams at the center of the antiHelmholtz coils. In each of the pairs the beams are counterpropagating with one beam being left circularly polarized (denoted σ^-) and the other right circularly polarized (denoted σ^+) shown in Fig.3.3.

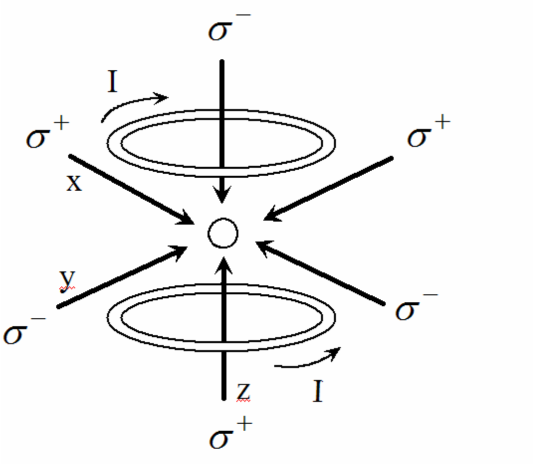

Figure 3.3: Schematic of a MOT. Six beams along 3 perpendicular axes are used along with two magnetic coils in antiHelmholtz configuration. Of each beam pair one beam is left circularly polarized (σ^-) and the other right circularly polarized (σ^+). The trapping region is formed at the intersection of the six beams.

Assume for illustration that the light is tuned below a transition from $F = 0$ to $F' = 1$ energy level. Fig.3.4 shows how the $m_{F'} = -1$ and $m_{F'} = 1$ levels are Zeeman shifted oppositely proceeding away from the center of the magnetic field coils (z=0). As discussed in section 2.3.2 $\sigma^{\pm}$ light induces transitions from $m_F = 0$ to $m_{F'} = \pm 1$. Hence atoms situated at positions of $z > 0$ will preferentially absorb light from the σ^- beam whose direction of propagation is towards the region of zero magnetic field. The opposite is true in the negative z direction where the Zeeman shifts are such that the m_F to $m_{F'} = +1$ transition is tuned closer to resonance so that the σ^+ beam is preferentially scattered by the atoms. These atoms are, again, pushed towards the region of zero magnetic field. This effect serves both to cool atoms and to confine them in the center of the MOT where the magnetic field is zero. The three pairs of beam provide confinement in all directions. The principle here is different than for the case of the optical molasses: in a molasses the atoms are slowed based on their velocity whereas in a MOT there is an additional spatially dependent force on the atoms which provides the trapping.

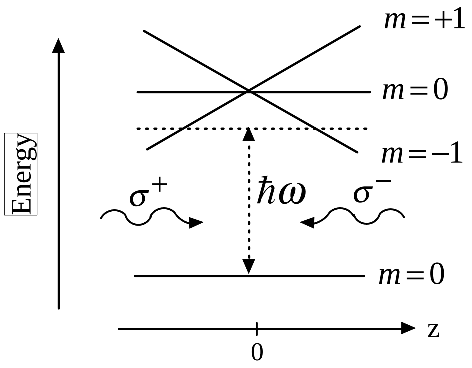

Figure 3.4: Focusing on one of the three beam axes we see the presence of the magnetic field Zeeman shifts the $m = +1$ and $m = -1$ excited hyperfine levels oppositely in opposite directions. $\sigma^{\pm}$ light drives transitions from $m = 0$ to $m = \pm 1$ so that when $z > 0$ the atoms preferentially absorb from the σ^{-} light and from σ^{+} light when $z < 0$). This drives the atoms towards the position of zero magnetic field strength. The light frequency shown in the figure is ω.

Temperatures on the order of 10-100 μK can be attained in a MOT with a limit on the minimum temperature being imposed by heating due to the random velocity fluctuations from aborption and spontaneous emission events.

3.3 Specifics to our lab

3.3.1 Energy levels

Alkali atoms are usually chosen for cooling and trapping given that the light frequencies needed typically coincide with commercially available laser products. The transitions used are $5^2S_{1/2}$ to either $5^2P_{1/2}$ or $5^2P_{3/2}$ named the D1 and D2 lines respectively. In the QDG lab we have constructed a MOT capable of trapping ^{6}Li,^{85}Rb, and ^{87}Rb.

Figs.3.5-3.7 show the energy levels of the 5S and 5P states of these isotopes.

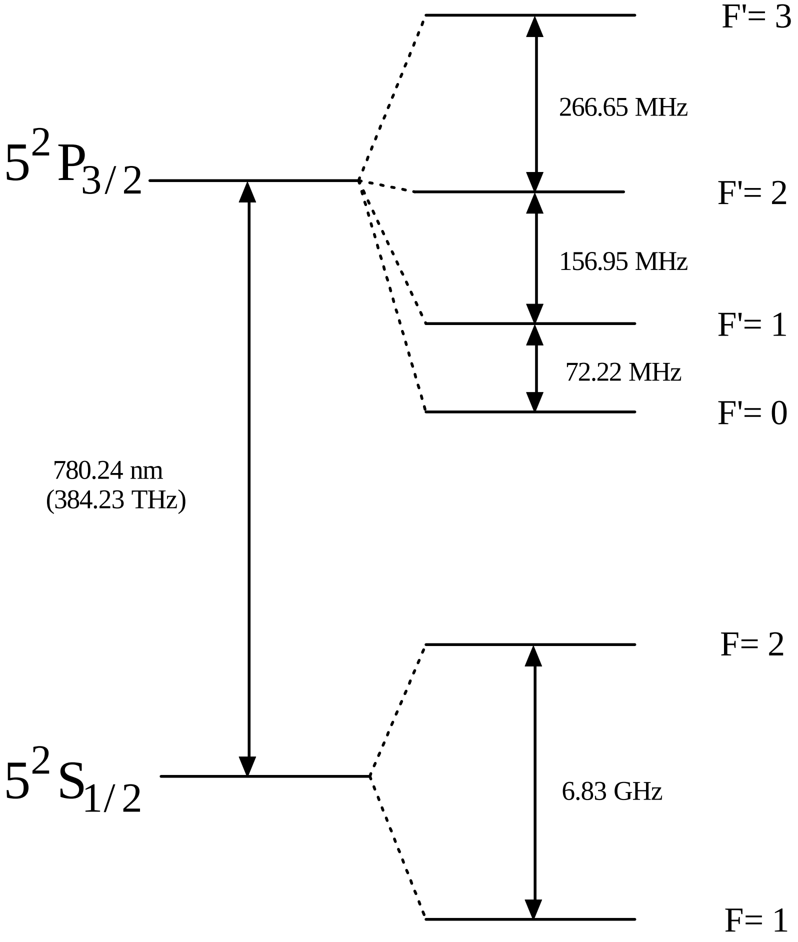

Figure 3.5: Hyperfine structure of the ^{87}Rb D2 transition in vacuum.

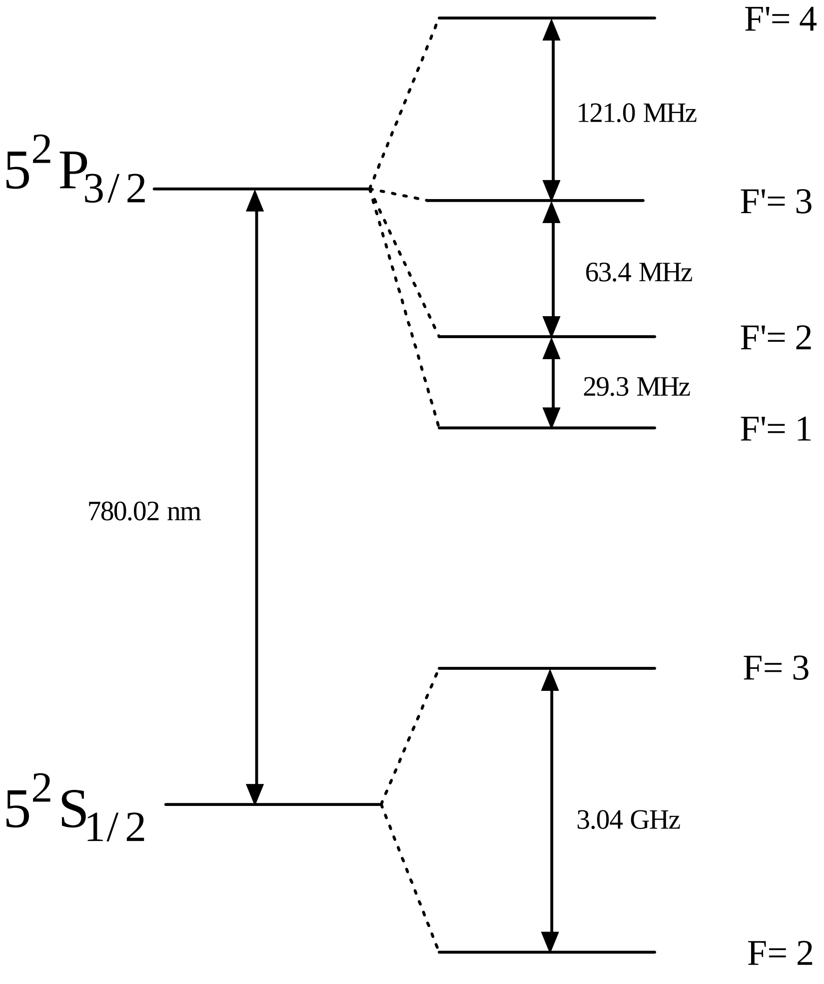

Figure 3.6: Hyperfine structure of the ^{85}Rb D2 transition in vacuum.

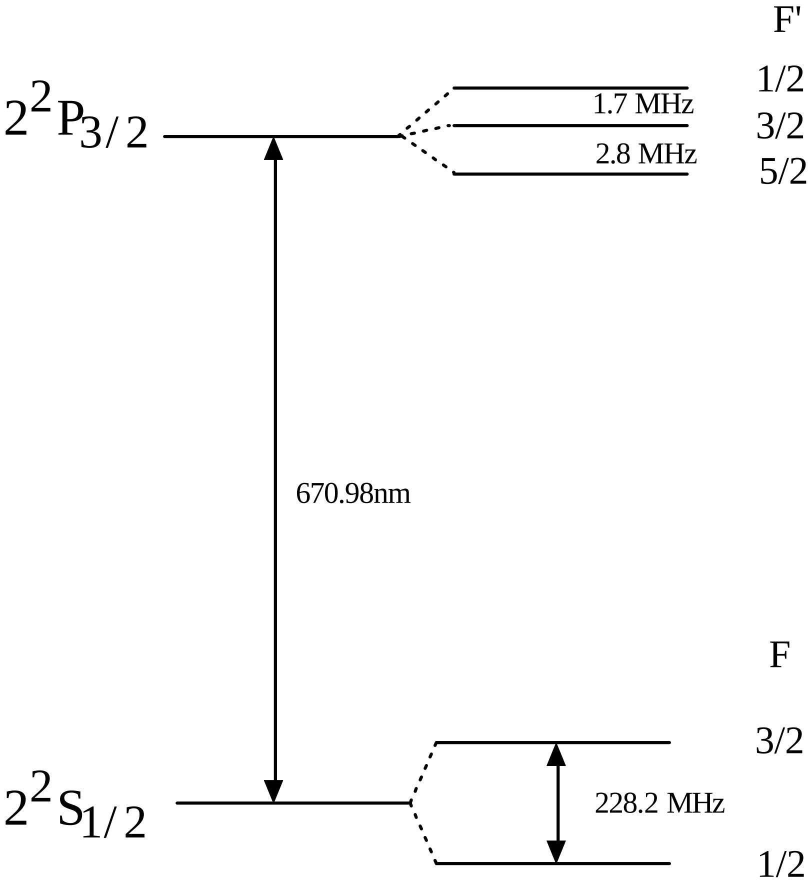

Figure 3.7: Hyperfine structure of the ^{6}Li D2 transition in vacuum.

3.3.2 Repumping

An important point not yet mentioned is that to succesfully cool and trap atoms in a MOT a secondary frequency is needed other than the light providing the cooling and trapping. Taking ^{85}Rb for an example, light that is red detuned from the chosen cooling transition ($F = 3$ to $F' = 4$) has a finite probability of exciting the ($F = 3$ to $F' = 3$) transition according to the selection rules allowing $F' - F = \pm 1, 0$. Atoms excited to the $F' = 3$ state can decay down to the $F = 2$ state putting it in a 'dark' state that the cooling light cannot access. The atoms quickly collect in this dark state preventing the formation of a MOT. To overcome this, some 'repump' light is added which optically pumps the atoms from the dark state back to the level accessible to the cooling light. The repump light may be tuned to the $F = 2$ to $F' = 3$ transition so that atoms collecting in the $F = 2$ state are excited to the $F' = 3$ state and preferentially decay to $F = 3$.

Table 3.1 shows the transitions chosen to use for laser cooling and the repump frequencies used.

	Cooling (F to F')	Repump (F to F')
^{87}Rb	$2 - 3'$	$1 - 2'$
^{85}Rb	$3 - 4'$	$2 - 3'$
^{6}Li	$3/2 - p/2'$	$1/2 - p/2'$

Table 3.1: Cooling and repump transitions used by the QDG lab. $p = 1, 3, 5$ for the hyperfine levels of ^{6}Li.

Cooling ^{6}Li is more challenging than cooling either ^{85}Rb or ^{87}Rb since the excited state hyperfine levels are closely spaced compared to the laser linewidth (2 MHz). This leads to a significant accumulation of atoms in the dark state, $F = 3/2$. In the case for $^{85/87}$Rb the repump light can be shone at the center of the MOT from any direction and a small power is needed, for the case of ^{6}Li however, the repump beams are shone from the same six directions as the MOT and with comparable intensity as that needed for the cooling beams.

3.4 Optical dipole traps

3.4.1 Principles and usage

In section 2.2.2 we saw the light shift depends on the electric field strength and therefore the intensity of the light, this implies that the light shifts will increase for increasing intensity of light that the atom is subjected to. This means if an atom originally in the atomic ground state $|1\rangle$ is subjected to a gradient in light intensity it will feel a force attracting it to the region of highest intensity for negative detuned light and conversely repelling it for positive detuning. This gives a more intuitive understanding of the origin of the dipole force, the physical mechanism upon which optical dipole traps (or dipole force traps) are based.

The light used for a dipole trap is far-detuned from atomic resonances to prevent heating from absorption. As a consequence the light from the the optical dipole trap does not cool the atoms, unlike in a MOT. Optical dipole traps are, however, used to cool the atoms beyond temperatures attainable in MOTs. This is acheived by the process of evaporative cooling. The intensity of the dipole trap is slightly lowered allowing the most energetic (hottest) atoms to leave (evaporate) from the trap. The remaining atoms rethermalize and the average temperature of the ensemble is decreased. Evaporative cooling allows one to reach temperatures well below (i.e below 1 μK) those attainable by laser cooling alone (between 10 and 1000 μK).

3.4.2 Gaussian Beams

The lasers used to generate the optical dipole trap typically output a Gaussian intensity profile. We will briefly review the properties of Gaussian beams and apply those properties to possible trap geometries. Please note that the discussion in the rest of this section is based on material from Refs. [ST91, GWO00].

The transverse cross section of a gaussian beam has an intensity distribution that is a circularly symmetric Gaussian function.

$$I(\rho, z) = \frac{2P}{\pi W^2(z)} \exp\left[-\frac{2\rho^2}{W^2(z)}\right] \tag{3.1}$$

where ρ is the radial distance and P is the power of the beam. The z axis is the axis at the center of the beam pointing in the direction of beam propagation and $W(z)$ (the beam radius) is the radial distance from the axis at which the intensity drops down to $1/e^2$ of its maximum value at the axis. The intensity of the beam is related to the electric field amplitude by $I = 2\epsilon_0 c|\mathbf{E}^+|^2$ where $\mathbf{E}^+$ again is the part of the electric field involving e^{iwt} from Eq. 2.23.

Fig.3.8 shows the axial behaviour of the $W(z)$ with respect to the z axis given by

$$W(z) = W_0 \left[1 + \left(\frac{z}{z_0}\right)^2\right]^{1/2} \tag{3.2}$$

W_0 is the min value of $W(z)$ situated at $z = 0$. The Rayleigh range $z_o = \frac{\pi W_0^2}{\lambda}$ is the axial distance at which $W(z)$ is $\sqrt{2}W_0$.

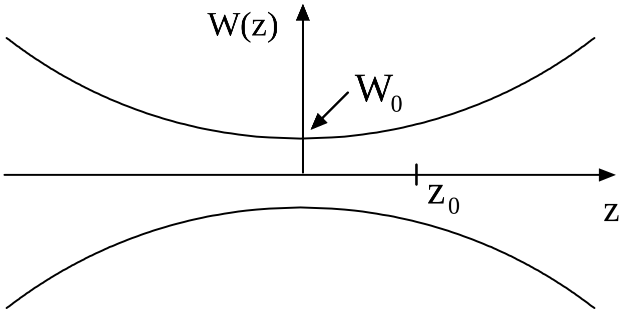

Figure 3.8: The beam radius of a gaussian beam $W(z)$ plotted as a function of the axial position z. W_0, the minimum beam radius, is called the waist of the gaussian beam. z_0, the Rayleigh range, is the z value at which $W(z) = \sqrt{2}W_0$.

The radius of curvature of the wavefronts of the gaussian beam is

$$R(z) = z \left[1 + \left(\frac{z_0}{z}\right)^2\right] \tag{3.3}$$

and at $z >> z_0$ the wavefronts are approximately spherical with $R(z) \approx z$.

3.4.3 Trap Geometry

Single pass trap

One possibility is to trap atoms at the focus of an intense laser beam. The light shift given in Eq.[2.70] defines the potential U that the atoms in ground state $|F, m_F\rangle$ are subject to with the trap depth U_T being defined as the maximum of that potential. For a focused gaussian beam that trapping region is centered around the waist of the beam and the maximum potential would occur at $\rho = 0$ and $z = 0$. Note that the intensity gradient is steeper in the radial direction than the axial direction.

For thermal energy $k_B T$ of the atoms much smaller than the trap depth the atoms will be confined to region well within the waist and Rayleigh range of the beam. The potential experienced by the atoms can then be approximated as being a cylindrically symmetric harmonic oscillator potential given by

$$U \simeq -U_T \left[1 - 2\left(\frac{\rho}{W_0}\right)^2 - \left(\frac{z}{z_0}\right)^2\right] \tag{3.4}$$

The radial and axial trap frequencies, ω_ρ amd ω_a for atoms of mass m are then

$$\omega_\rho = \sqrt{\frac{4U_T}{mW_0^2}} \tag{3.5}$$

$$\omega_a = \sqrt{\frac{2U_T}{mz_0^2}} \tag{3.6}$$

Standing wave trap

Another possible trap geometry is a 'standing wave trap' constructed by retro-reflecting back the light with a spherical mirror so it refocuses back at the waist or by using an optical resonator in which the light is reflected and forth between mirrors creating an effective amplification in the initial input intensity. The atoms will be trapped in the periodic positions of highest intensity of the standing waves(see Fig.3.9). With the same assumptions of spatial confinement mentioned above the potential experienced by the atoms can be expressed as

$$U \simeq -U_T \cos^2(kz) \left[1 - 2\left(\frac{\rho}{W_0}\right)^2 - \left(\frac{z}{z_0}\right)^2\right] \tag{3.7}$$

where $k = 2\pi/\lambda$.

The trap depth for the standing wave trap will be 4 times larger than for the single focused beam trap described above. Standing wave traps are not necessarily ideal for evaporative cooling due to tunnelling of the atoms axially along the periodic lattice [Joc04]. An alternative is to initially load

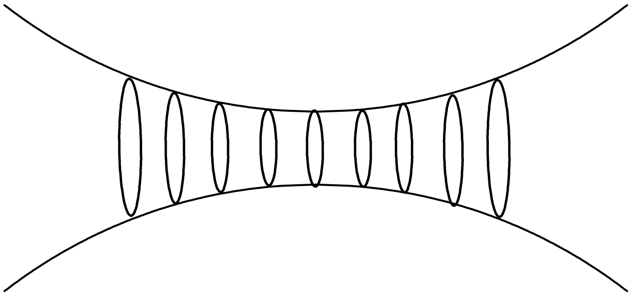

Figure 3.9: Atoms trapped in a standing wave trap will be distributed at periodic positions formed from local intensity maxima.

the atoms from a MOT into a standing wave trap to capture a large number of atoms and then transfer the atoms into a single focus dipole trap for evaporative cooling.

3.4.4 Loss Mechanisms

Spontaneous emission

Atoms in the excited atomic states $|2\rangle$ will be repelled from regions of high intensity for negative detuning and attracted for positive detuning. The presence of spontaneous emission can complicate trapping of atoms using a dipole force. This occurs because spontaneous emission can occur between adjacent manifolds of the dressed state eigenstates. Fig.3.10 shows the transitions for which spontaneous emission occurs between two energy manifolds for $\Delta < 0$. Spontaneous emission provides a mechanism for loss in the number of atoms trapped since if an atom is in the trappable $|\psi_-(n)\rangle$ state (for $\Delta < 0$) it can decay to the untrappable $|\psi_+(n-1)\rangle$. The atom will then again quickly decay to a trappable state, however, the atom momentarily experienced a repulsive potential which serves as a heating mechanism. Even if the atom decays directly to the trappable $|\psi_-(n-1)$ state the process of spontaneously emitting a photon contributes to heating of the atoms due to the momentum imparted to the atoms upon emission.

Heating of the trapped atomic sample can also occur by the scattering of light described by the scattering rate at which atoms absorb and re-emit photons from the trap light. For a two level atom the scattering rate is

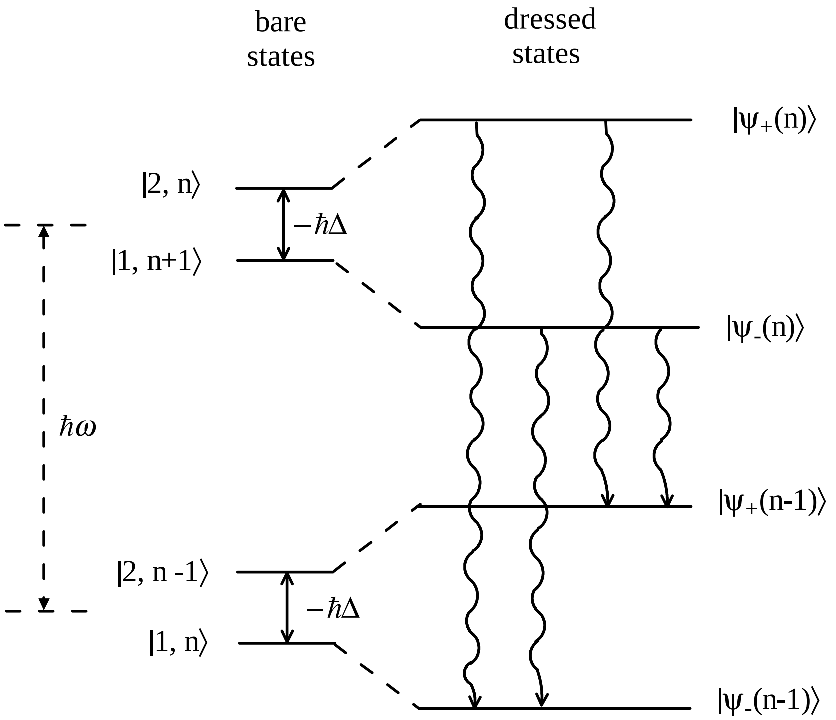

Figure 3.10: Spontaneous emission between two energy manifolds for $\Delta < 0$. The $\psi_+(n)$ and $\psi_+(n-1)$ states are untrappable since atoms in these staes will be repelled from the trap. Even if decay occurs into a trappable state, heating from photon emission occurs.

related to the optical potential experienced by the atom by

$$\hbar\Gamma_{sc} = \frac{\Gamma}{\Delta}U \tag{3.8}$$

where Γ is the spontaneous decay rate.

For multilevel atoms the scattering rate of atoms in ground state g is given by

$$\Gamma_{sc} = \frac{\Gamma}{4\hbar}\sum_e |\mathbf{d}_{eg}\cdot\mathbf{E}|^2\left[\frac{1}{(\omega_{eg}-\omega)^2}\right] \tag{3.9}$$

using the potential given by Eq.[2.70] disregarding the $1/(\omega_{eg}+\omega)$ term which is small compared with the difference term. The heating rate $\dot{T}$ due to this scattering can be expressed as [GWO00]

$$\dot{T} = \frac{2}{5}\frac{\hbar^2 k^2}{m}\Gamma_{sc} \tag{3.10}$$

The light in an optical dipole trap is far-detuned to minimize this heating mechanism.

Collisions

Collisions are another mechanism whereby atoms leave the trap. The decay of the number of atoms from the trap can be described by

$$\frac{dN(t)}{dt} = -\alpha N(t) - \beta \int n^2(\mathbf{r},t)d^3r - \gamma \int n^3(\mathbf{r},t)d^3r \tag{3.11}$$

where $n(\mathbf{r},t)$ is the atomic density. The first term in Eq.[3.11] characterizes the loss due to collisions of the trapped atoms with the background gas. Ref. [GWO00] estimates the lifetime of atoms in the trap before being lost to this type of collisions is $\sim$ 1s at a pressure of 3×10^{-9}mbar. The second term accounts for collisions involving two trapped atoms. In this case if the atoms are not in their absolute ground state upon an inelastic collision the state of the atoms may change, releasing energy into their kinetic motion and causing them to leave the trap. In particular spin-changing collisions such as hyperfine-changing collisions where the atoms in an upper hyperfine state decay to the lower hyperfine ground state are of this type. The third term describes three-body losses which potentially lead to two atoms forming a dimer and the third atom acquiring the energy released from the dimer formation. This results in all three atoms leaving the trap.

Chapter 4

The Master Table

4.1 Overview

The purpose of the master table is to generate frequency stabilized laser light to be sent to experimental tables where magneto-optic traps are constructed and experiments with ultra-cold atoms can be performed.

At one end of the master table there are five external cavity diode lasers (ECDLs). Four of these five generate cooling and repump light for the two isotopes of Rb and one produces light for ^{6}Li. Fig.4.1 shows ECDLs and labels their usage as well as the optical components in use. The ECDLs lie on a separate bread board separated from the main table by lead lined foam and there is a plastic enclosure also lined with the same type of foam. Holes are drilled out of the front to let the light out.

After each ECDL is one or two optical isolators to protect them from back reflections. The light from each ECDL is periscoped down to the level of the table with $\sim$ 20 mW coming from each Rb ECDL and $\sim$ 3 mW from the Li ECDL. Most of the ECDL power is used in a saturated absorption setup while $\sim 1-2$ mW is sent to a secondary laser which outputs the same frequency as the ECDL but at a greater power essentially amplifying the master light. These amplifying lasers are called 'slaves' and the ECDLs are called 'masters', hence the optical table is called the 'master table'.

The light from each of the slaves is coupled into optical fibers. The light from these fibers is distributed to the experiment tables and to the diagnostics. These diagnostics serve to verify that the slaves are properly injected by the masters.

This chapter will describe how the masters are frequency stabilized, the setup for injection, how to use the diagnostics, as well as issues that arose during the process of making this table functional and how these issues were resolved.

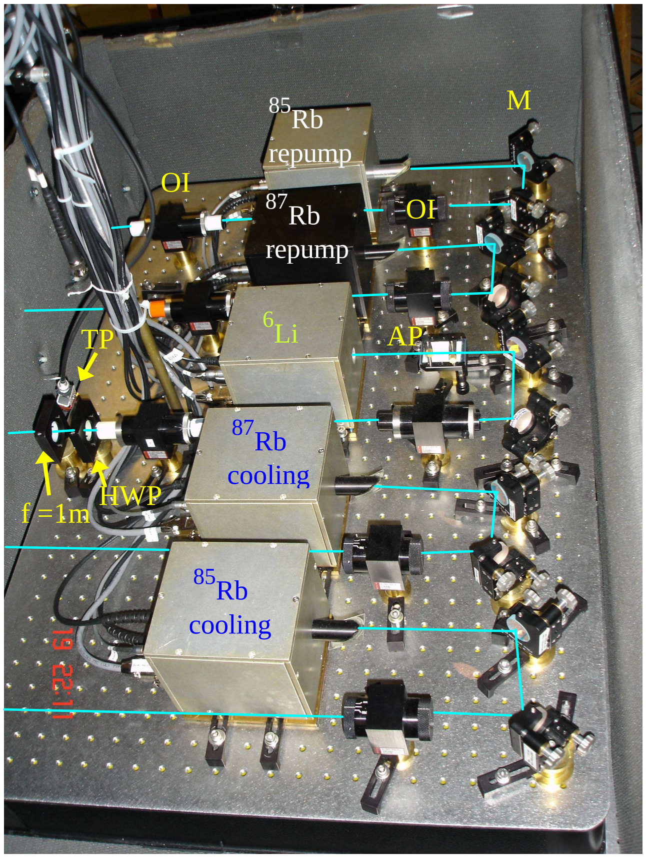

Figure 4.1: The light from each ECDL is directed into an optical isolator (OI) by two mirrors (M). One or two optical isolators may be used. The four ECDLs for Rb are shown, two for the ^{85}Rb and ^{87}Rb repump light and two for the cooling light. There is one master for ^{6}Li. The Li ECDL setup includes an anamorphic prism pair (AP) for beam shaping and also a half wave plate (HWP) and $f = 1m$ lens due to space constrictions on the main table. A temperature probe(TP) is used to monitor the temperature inside the enclosure.

4.2 Frequency stabilization

4.2.1 ECDLs

As previously mentioned, the intial starting point of the light generation is from external cavity diode lasers (ECDLs). Semiconductor laser diodes are inexpensive and easy to use, a drawback being that their output has a large frequency linewidth(∼100 MHz) [AWB98]. To select and narrow the frequency output by the diodes a grating is placed external to the laser diode to reflect the first diffracted order back into the laser diode with the angle of the grating determining the frequency fed back. The feedback will saturate the gain medium extinguishing competing frequencies in the laser diode. The laser diode itself consists of a cavity containing a gain medium, with the presence of the grating adding an external cavity formed between the grating and the back face of the laser diode internal cavity. The diode laser's temperature and the injection current change the cavity length of the laser diode thereby changing which frequencies are resonant with the cavity. The temperature and the current are tuned so that the frequency mode fed back into the laser diode from the grating is resonant both with the internal and external diode cavities then the laser will output a single narrow frequency sent back by the grating.

Fig.4.2 shows our ECDL design based on a design given by Ref. [HWS01]. This design has the property that the direction of the output laser beam is not affected by the frequency of the light being sent back by the grating. This is acheived by mounting a mirror on the same mounting piece to which the grating is mounted so that it compensates for changes in the grating angle. The frequency of the semiconductor laser diode can be continuously selected by the presence of piezoactuators (piezos) that change the position and angle of the grating. The temperature is controlled by a thermoelectric cooler placed under the laser mount and the current is supplied by a current controller whose output is first sent through a protection circuit in the ECDL box before being sent to the laser diode. The temperature being a parameter that is slow to change it is kept constant at all times at a fixed value. The current and the position of the piezos have a much faster response time so they are actively controlled to keep the ECDLs stable at a single frequency. The construction of the ECDLs is described in detail, in Ref. [KE05] with useful additions given in [Sin07]. The latter of which also contains a comprehensive list of which commercial laser diodes we use in the QDG lab.

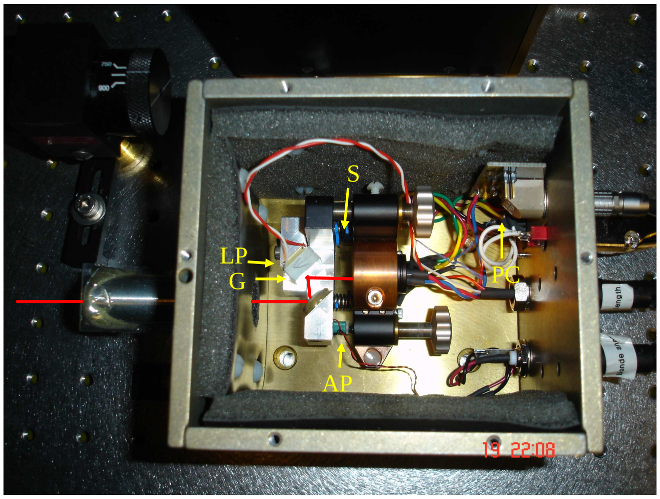

Figure 4.2: Design of an EDCL. Before leaving the ECDL box the light from the laser diode mounted in a modified mirror mount reflects off of the grating(G) and a mirror. One piezo (LP) is placed behind the grating to change the length of the external cavity formed between the grating and the semiconductor laser diode back facet. Another piezo(AP) is placed at the horizontal control knob of the modified mount to change the angle of the grating to select the frequency output. A thermoelectric cooler is underneath the bottom of the modified mirror mount to control the temperature of the laser diode. The current sent to the laser diode is passed through a protection circuit (PC) to prevent damage to the laser diode. Sorbathane pads(S) are placed in between the springs of the mount to dampen vibrations.

4.2.2 Saturated absorption locking

Principle

Saturated absorption spectroscopy is used to provide the signal needed to monitor and control the frequency of the laser. Fig.4.3 shows the optical setup needed for saturated absorption spectroscopy.

In this setup, light from a master laser is sent in counterpropating directions through a Rb or Li vapour cell. In one direction the master light is collected on a photodiode giving an absorption signal, this beam of light is called the probe beam. A more intense counterpropagating pump beam travels through the cell overlapping the probe beam. If frequency of the pump and probe beam, ν, is equal to an atomic resonance then the atoms will absorb from both the probe and the pump.

Without the pump beam, the absorption signal from the probe beam as ν changes follows a Doppler-broadened Lorentzian shape called a Voigt profile. Fig.4.4 shows the absorption profiles from ^{85}Rb and ^{87}Rb with no pump beam. The presence of the pump beam results in appearance of sharp dips in the absorption profiles at frequencies corresponding to resonances for velocity classes of atoms that can absorb from both beams.

Focusing on the ^{87}Rb $5^2S_{1/2}$, $F = 2$ to $5^2P_{3/2}$ absorption profile as an example we would expect expect 3 dips for $F = 2$ to $F' = 1, 2, 3$. Fig.4.5 shows the actual probe absorption profile in the presence of the pump, though a little difficult to tell by eye there are actually six dips. The extra dips are due to 'crossover resonances' which correspond to transitions from ($F = 2$ to half way between $F' = 1$ and $F' = 2$, $F' = 2$ and $F' = 3$, $F' = 1$ and $F' = 3$). These crossover resonance frequencies occur because when the pump and probe frequency have these frequencies atoms that are travelling with the appropriate velocities will see the pump light shifted to one resonance and the probe light shifted to another so that those atoms can still absorb from either the pump or the probe simultaneously.

From the saturated absorption setup used on our master tables for one of the four Rb masters shown in Fig.4.3 we see the beam to be used for the pump beam is focused and passes through an acousto-optic modulator(AOM) before reaching the Rb atoms in a cell containing a 50/50 mixture of Rb 85 and Rb 87. The AOM serves to shift the frequency of the pump with respect to the probe, this has the effect of shifting the positions of the peaks relative to their position when the pump and probe frequencies are the same. If the pump has a frequency $\pm\delta$ relative to the probe beam the saturated absorption dips will be shifted by $\mp\delta/2$. Being able to set

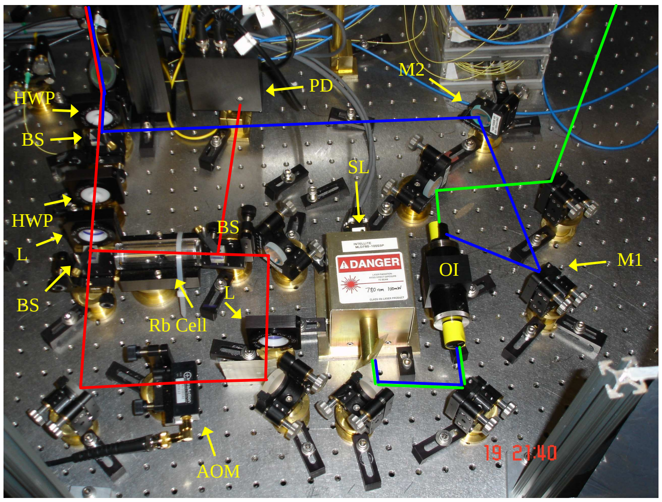

Figure 4.3: A saturated absorption and slave injection setup for one of the Rb ECDLs. The red and blue lines indicates the path of the light used for the saturated absorption and slave injection setups respectively. The green line shows the path of the light coming from the slave laser(SL). The light from the master initially is taken down to the level of the table using a periscope and passes through a halfwave plate(HWP) and beam splitting cube (BS) which is used to send a variable amount of light to the setups for saturated absorption and slave injection. For the saturated absorption setup the light is again split with a HWP and BS to form the pump and the probe beam. Before being sent to the Rb cell the pump beam passes through an acousto-optical modulator (AOM). The probe beam bounces off a beam splitting cube and is sent to a photodetector(PD). The signal from the photodetector provides information on the amount of probe light being absorbed in the Rb cell which contains a gas of ^{85}Rb and $^{87}\mathrm{Rb}$. L in the figure indicates lenses. For the slave injection setup the master light is steered into the side port of an optical isolator using mirrors M1 and M2 and is used to inject the slave laser. The light from the slave passes through the isolator and is sent to be coupled into a fiber network.

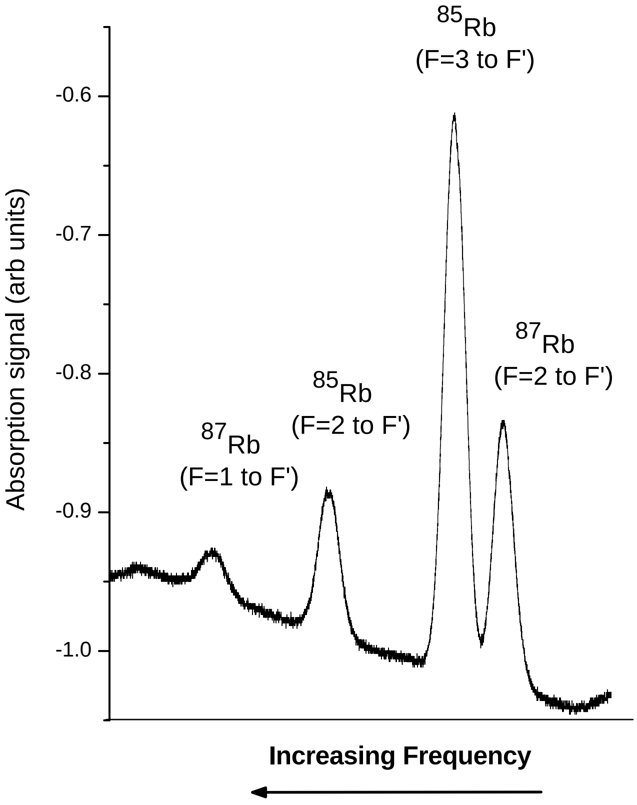

Figure 4.4: A plot of the probe absorption signal for Rb as a function of master frequency with the pumb beam blocked. The absorption profiles are due to the transitions from the two hyperfine ground states to the excited hyperfine states of the D2 transition for ^{85}Rb and ^{87}Rb. The absorption profiles do not appear as sharp lines due to the doppler shifting of the light by different velocity classes of the atoms.

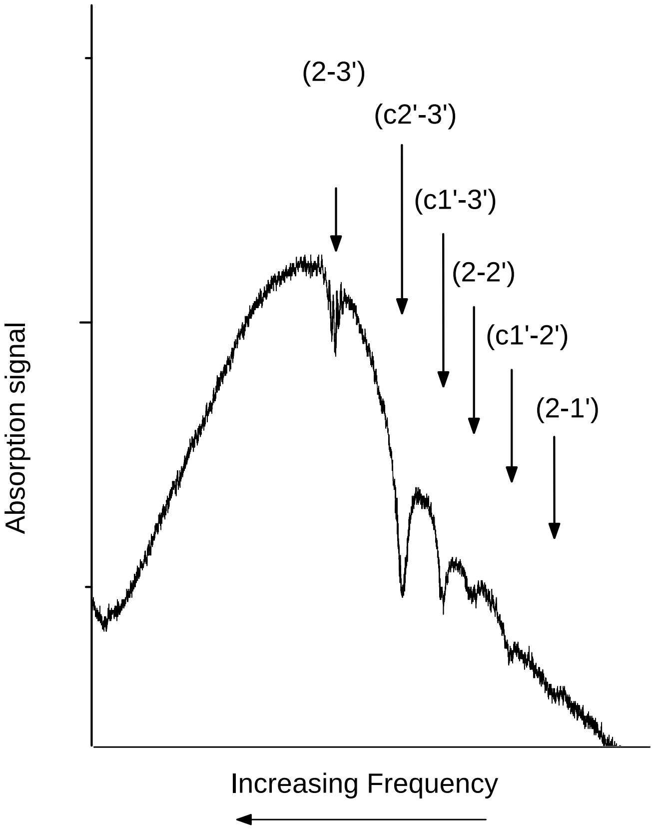

Figure 4.5: An absorption profile with saturated dips. The overall profile is a zoomed in version of the Rb 87 $5^2S_{1/2}$, $F = 2$ to $5^2P_{3/2}$ profile shown in Fig.4.4. With the presence of the pump there are six saturated absorption dips due to the transitions from the $F = 2$ to $F' = 1, 2, 3$ denoted (2-1'),(2-2'),(2-3') and from the crossover resonances from $F = 2$ to halfway between $F' = 1, 2, 3$ denoted (c1'-2'),(c1'-3'),(c2'-3').

where the dips are gives the ability to choose a convenient place at which the masters are locked.

Usage

The signal from the probe beam is fed into electronic equipment (the 'lock box') which generates an error signal that is proportional to the derivative of the absorption signal. Fig.4.6 shows the error signal generated corresponding to an input into the lock box of a saturated absorption signal from the probe sweeping over the Rb 87 $5^2S_{1/2}$, $F = 2$ to $5^2P_{3/2}$, $F' = 2 - 3$ crossover resonance.

At the saturated absorption peaks the error signal will be zero right at the minimum of the dip and be rapidly rising with opposite sign on either side of the dip minimum. The error signal provides a means for the stabilization of the master frequency. If the frequency sweep of the ECDL is reduced to zoom in on one of the saturated absorption peaks(as shown in Fig.4.6) then the error signal will consist only of a zero and a positive and negative voltage. Once the frequency sweep is completely turned off (by not sweeping the piezo positions and the current) and the feedback control of the lock box is enabled, the lock box will control the position of the grating via the piezoelectric elements and the injection current to keep the error signal at zero. At this point the master is 'locked'.

4.3 Locking schemes

Usually the most prominent saturation dip is used to lock the master laser frequency since this generates the largest error signal. However any feature that has an associated error signal large enough for the lock circuit to be able to sense where zero is will work. Figs.4.7, 4.8 and 4.9 show the saturated absorption dips and the error signals that the Rb and Li masters are locked to. The particular place we lock to is shown by the 'lock here' arrows. Zero on the diagrams on the right indicate the frequency we will use for the cooling of the Rb isotopes(shown in Table.3.1). All the other frequencies listed are in MHz and are relative to the zero position. The saturated absorption dip responsible for the error signal to which we lock is written in blue. Because of the presence of the AOM in the saturated absorption setup, the actual frequency of the saturated dip we lock to is shifted (written in red). The frequency output by the master laser corresponds to this shifted frequency. The frequencies are later shifted to be below the atomic transitions. This shifting at each experimental step allows the actual experimental frequencies

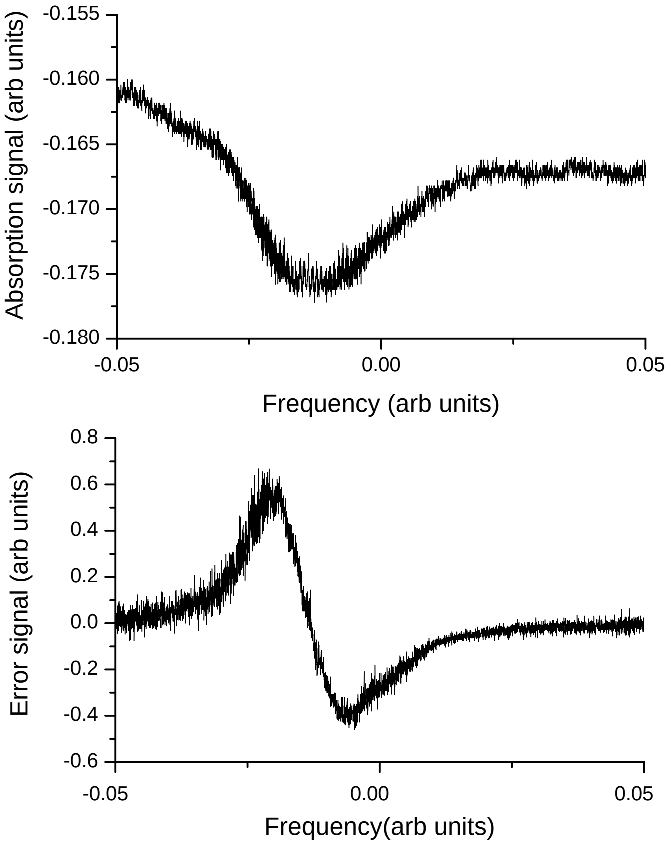

Figure 4.6: The error signal (lower panel) is shown corresponding to a saturated absorption dip(upper panel) for the Rb 87 $5^2S_{1/2}$, $F = 2$ to $5^2P_{3/2}$, $F' = 2 - 3$ crossover resonance. Note that the error signal is zero at the minimum of the saturated absorption dip and rapidly rises with opposite sign on either side of the zero. When the ECDL is locked to this error signal the frequency sweep is disabled and the piezo elements inside the ECDL and the current of the ECDL are controlled so that the error signal is kept at zero.

used to vary while the masters are always locked to the same frequencies. The system was designed so that Rb master laser frequencies are locked 180 MHz below the experimental frequencies.

For Li we cannot distinguish the saturated absorption dips for each hyperfine level but see 3 dips corresponding to the transitions from the two ground states of $2^2S_{1/2}$, $F = 1/2$ and $F = 3/2$ to the excited levels of $2^2P_{3/2}$ and a crossover betweeen those two transitions. Li also has a slightly different setup than Rb in that the shifting of the frequencies to the correct experimental frequencies occurs on the master table (see the next section 4.5 for further details).

Table 4.1 summarizes the frequencies used for the AOMs in the saturated absorption set ups (called the lock AOMs) which determines the frequency at which the masters are locked.

Laser	Lock AOM Frequency (MHz)	AOM order
^{85}Rb cooling	120	+1
^{87}Rb cooling	94	+2
^{85}Rb repump	103	+2
^{87}Rb repump	101	+2
^{6}Li	88	+2

Table 4.1: Frequencies used for the lock AOMs in the saturated absorption setups. The RF frequency sent to drive the AOMs determines at which frequencies the masters are locked. The AOM order column indicates which diffracted order is used of the light when passing through the AOM. The (+2) order beam is shifted up by 2 times the AOM frequency as compared to the incoming light.

4.4 Amplification

Though the masters have the ability to be frequency stabilized their output power is not sufficient to be used for laser cooling and trapping. Most of the power from a master is used for the saturated absorption locking and the remainder ($\sim$ 1 mW) is sent into another higher power diode which outputs $\sim$ 60 mw for the Rb slave laser diodes, and $\sim$ 25 mW for the Li diodes. Ref. [Sin07] has a complete list of the diodes used for the masters and the slave amplifiers.

When light from the master is sent into the gain medium of the higher

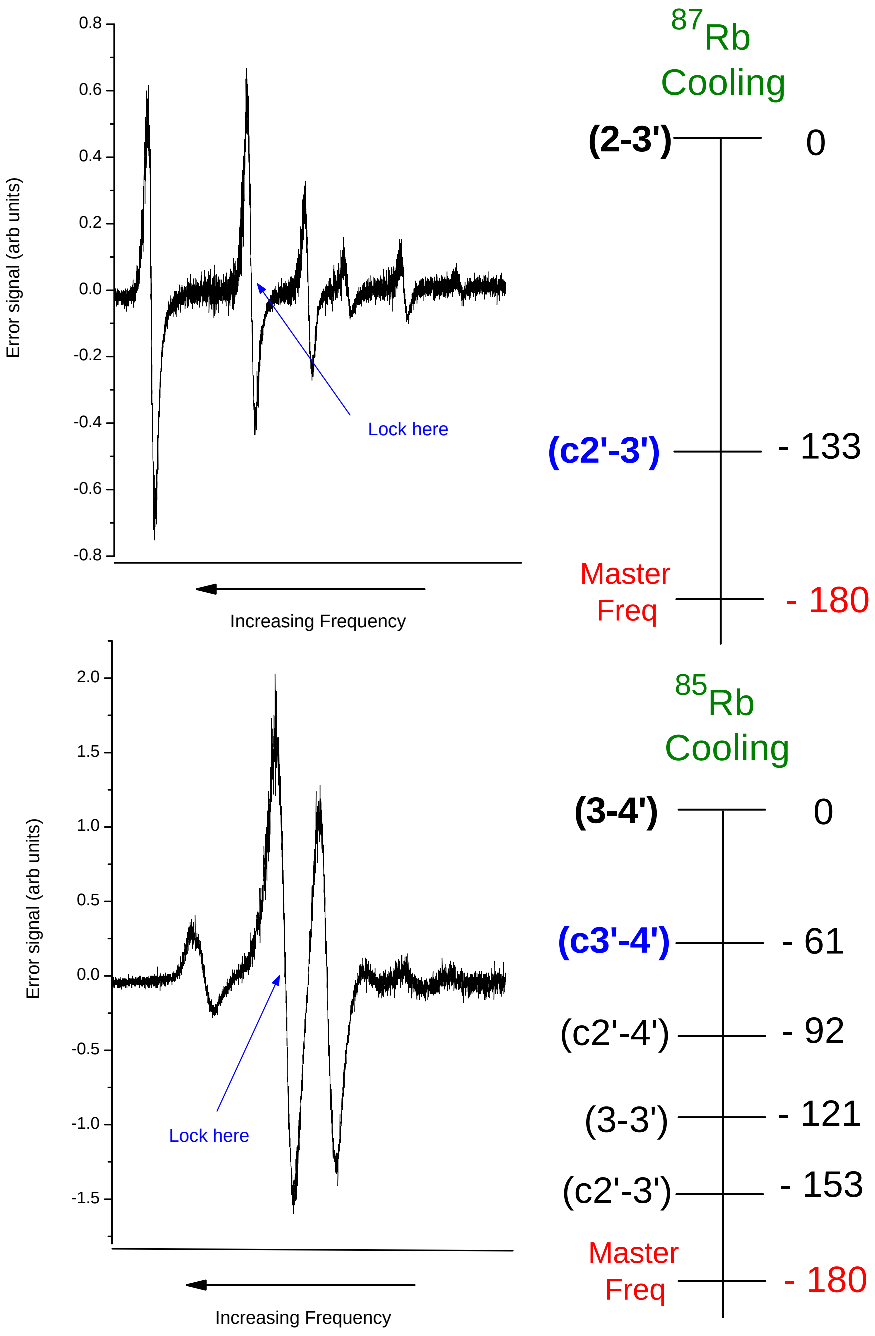

Figure 4.7: The error signals and locking schemes for the Rb cooling lasers.

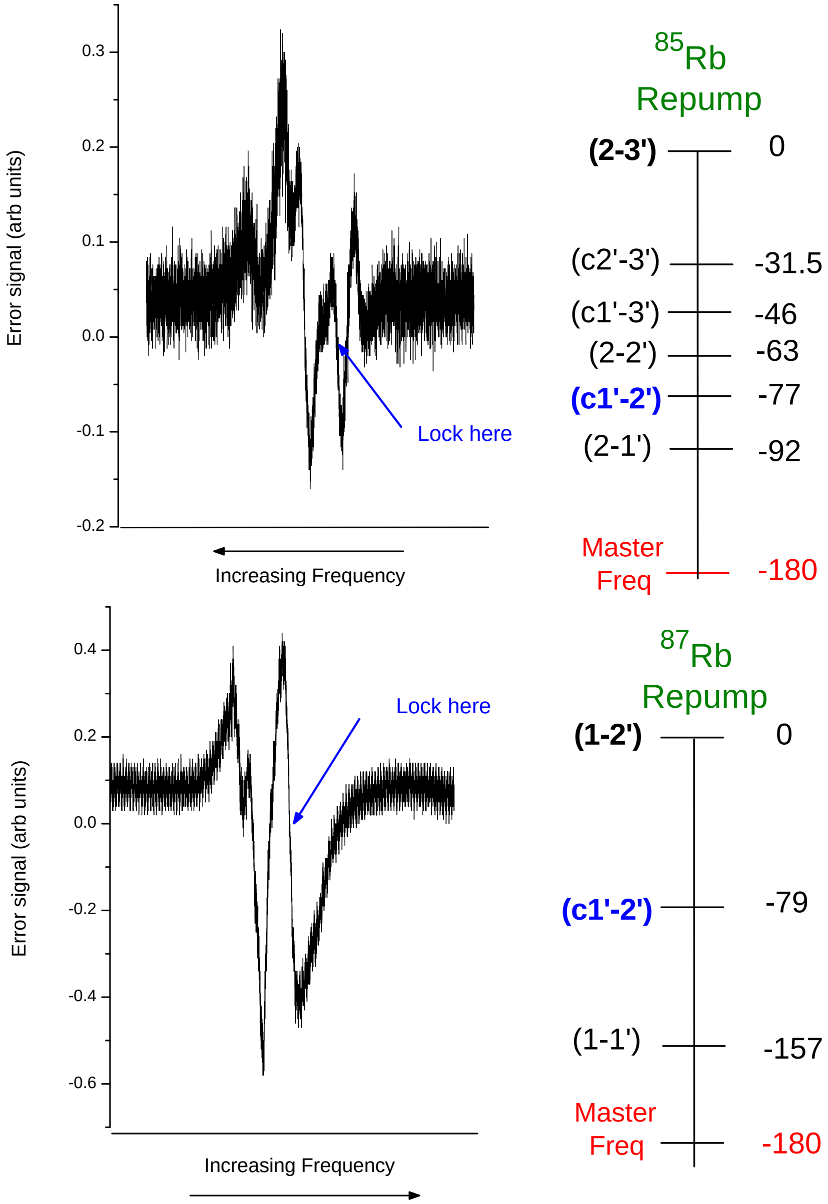

Figure 4.8: The error signals and locking schemes for the Rb cooling lasers.

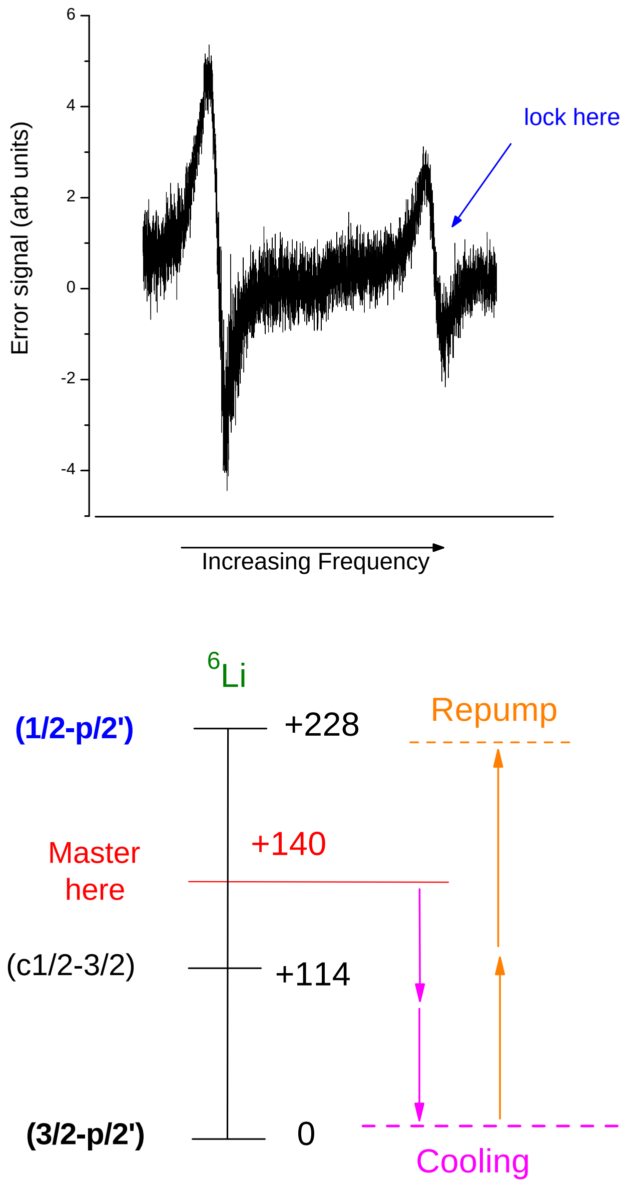

Figure 4.9: The error signal and locking schemes for the Li master laser. The pink and orange dashed lines indicate the frequency needed for the cooling and repump light respectively (exact frequencies are not given since that is variable). The arrows indicate that the light is shifted by the AOM double passes described in Fig.4.13. p indicates the excited hyperfine levels.

power diode, the master light saturates the gain medium and extinguish competing modes [Had86] so that the slave outputs only the master frequency at its natural power. This technique is called *injection locking.* Fig.4.3 shows the optical setup used on the master table for injection locking. The injection beam from the master is sent to the slave by the side port of an optical isolator which additionally protects the slave from back reflections. The polarization of the injection beam is vertically polarized so that it reflects off of a Glan-Thomson polarizer inside the isolator and is sent into the slave diode. Ref. [Sch07] provides excellent detail concerning the slave injection process, with a brief review presented here.

4.4.1 Injection procedure

4.4.2 Temperature tuning

When first setting up a slave it is useful to diagnose its output using an optical spectrum analyzer or monochromator to determine the slave's free running frequency. The slave's temperature (heat to increase wavelength) and injection current are adjusted so that the frequency is close to the intended master frequency to inject the slave. Fine tuning of the current will be needed later but the temperature will be kept constant. The free running wavelength of the Li slaves is quite far(658 nm) from where we inject them(671 nm) so that they needed to be heated close to their maximum possible temperature (we run them at 68 °C). The Rb slaves free running wavelength is within several nm above of the 780.2 nm light we inject them with and they are cooled to 18 °C.

4.4.3 Alignment

Important aspects of the alignment of the injection beam into the slave diode are that the injection beam should be aligned to the vertically polarized beam being rejected back through the side part from the slave light itself. It is important to first align the beam as best as possible by eye (when well aligned the rejection beam will go right back to the master). It is then useful to monitor the *Booth factor* which is the output power of the slave at the lasing threshold current with the injection beam present versus the output power without the injection beam. The fine tuning of the alignment occurs while 'walking' the injection beam to optimize the Booth factor. Two mirrors are required to align the injection beam into the slave and 'walking the beam' means turning the horizontal control knob of the mirror mount closest to the isolator in one direction (M1 in Fig. 4.3) and then optimizing the Booth factor with the horizontal control knob of the other mirror mount(M2). Continuing to change M1 in the same direction and reoptimizing with M2 will indicate if the Booth factor is going up or down which indicates whether to keep on changing M1 in the same direction or to go in the other direction. The same process is then repeated for the vertical control knob with iterative successions between changing the horizontal and vertical knobs until the maximum Booth factor has been achieved. If sufficient care has not been taken to align the beam by eye to begin with it is possible to align to a local maximum in the Booth factor which will not provide good slave injection.

4.4.4 Diagnostics and usage

On the master table also resides a Fabry-Perot(FP) and absorption cell for Rb and for Li to diagnose whether the slaves are injected (see Fig.4.10).

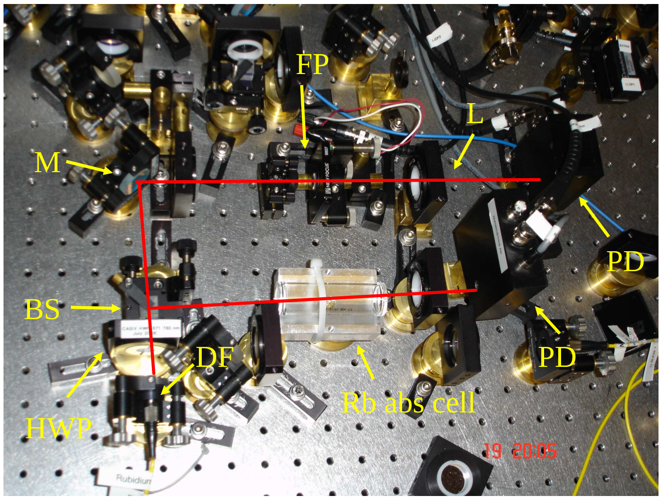

Figure 4.10: The diagnostic setup for the Rb slave amplifiers. The light from a slave amplifier is sent to fiber (DF) and is variably split by a half wave plate (HWP) and beam splitting cube (BS). The absorption signal of the slave is given by the amount of light incident on a photodector (PD) after passing through a Rb absorption cell (Rb abs cell). The light also passes through a Fabry-Perot with the transmitted light incident on a photodetector.

The Fabry-Perots serve to indicate the spectral purity of the slave beams and the absorption cells to determine whether the slaves are lasing at the same frequency as the master. The length of the FP cavities are ramped at 10 Hz so that a single frequency input shows multiple equally spaced FP peaks. Light is sent to the diagnostics though optical fibers. Fiber switchers (JDS FiTel SB and SC series) are used to select which light is sent to the diagnostic fibers.

To use the diagnostics to characterize the slave injection one can ramp the master frequency over a range containing the desired locking frequency. The slave's current is changed until the slave's absorption signal matches that of the master over some frequency range (approx 1.5 GHz for the Rb slaves). The current is fine tuned so that this window over which the slave follows the master contains the region with the frequency that the master will be locked to (see Fig.4.11). The frequency range over which the master is ramped is then decreased to zoom in on the saturated absorption feature to which the master is locked. The FP signal should sweep back and forth as the master frequency is swept and when the master is locked the FP signal should become stationary (modulo the motion caused by air currents). When injected the FP peaks should be sharp with a minimized noise floor(see Fig.4.12). Note that there are multiple current windows over which the slave is injected so that the current is tuned to a window where sufficient power is present for the desired application of the slave. For the Rb slaves these are separated by $\sim$ 25 mA and for Li $\sim$ 10 mA.

Slight differences in this procedure exist for the Rb and Li slaves as for Rb the absorption sweep is necessary since even when the slaves are not injected the FP peaks look sharp. One can still use the FP but if the master is locked and the peaks are clean looking it does not mean the slaves are injected. Ramping the master slowly over a small frequency range, one should see the peaks move back and forth if the slave is injected. For Li the absorption signal of the slaves is poor due to insufficient power (the Li fiber switcher has only $\sim$ 5 percent efficiency). We rely more on the FP since the FP signal when the slaves are not injected is very poor and noisy looking. If the master frequency is swept slightly the FP peaks should move back and forth gently and should be sharp looking. Sweeping the master is not completely necessary and one can just tune the current of the Li slaves until the noise floor goes down and the FP peaks grow taller and sharp.

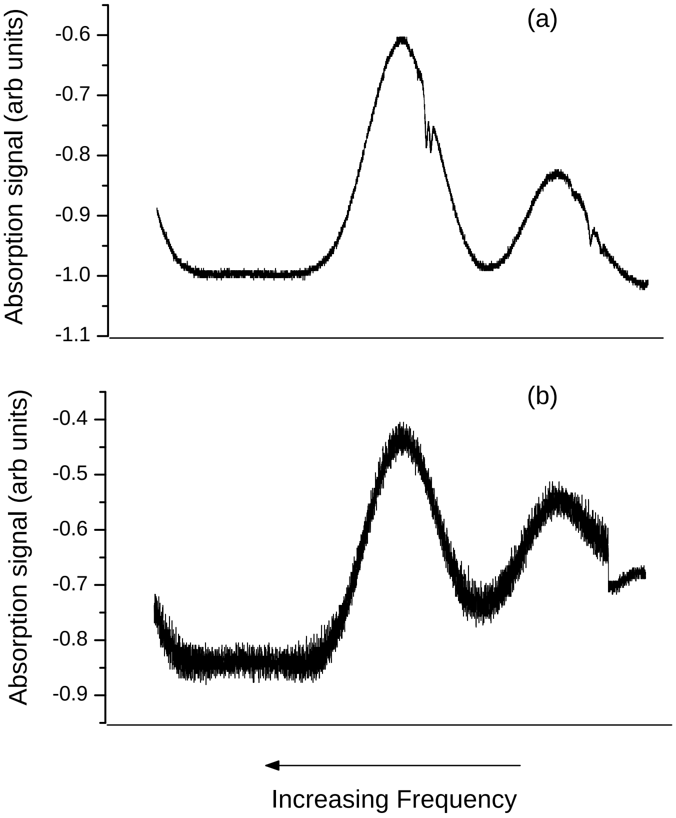

Figure 4.11: (a) Shows the absorption signal of a master and (b)shows the absorption of a slave injected by that master. The discontinuity in the slave absorption signal on the right indicates the slave is not following the master past that frequency. The center frequency and range over which the slave follows the master can be changed by changing the current of the slave.

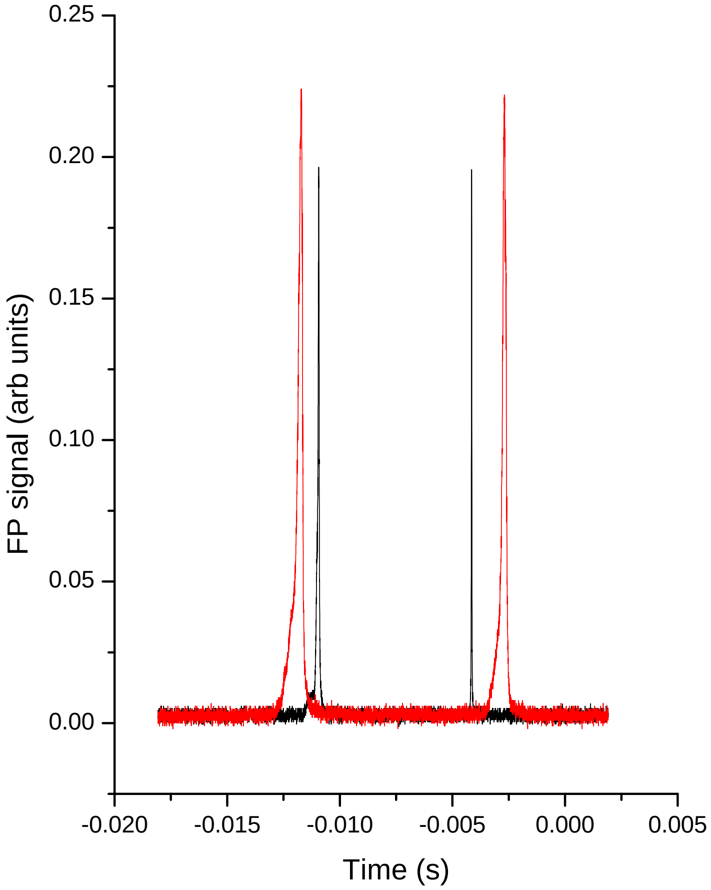

Figure 4.12: Fabry-Pérot (FP) traces of injected slaves for Li(red) and Rb(black) when the masters are locked. The relative position of the mirrors of the FP are scanned so that there are multiple transmission peaks as a function of time shown for a single frequency input. Sharp, equally spaced, and clean looking FP peaks with a flat noise floor indicates that the slave is properly 'injected'.

4.5 Usage of slave light from the master table

This section will provide further details to explain how the light generated on the master table is used towards the creation of $^{85/87}$Rb and ^{6}Li MOTs.

4.5.1 Rubidium

The output of the Rb slaves on the master table is coupled into fiber splitters where light is coupled into one fiber input and is split roughly equally amongst three fiber outputs. Light from these splitters is sent to experimental tables where a magneto-optical trap resides. One of the three fibers is used to send the slave light to the fiber switcher for diagnostic purposes. Having the slave light split means there is not sufficient power from the slaves on the master tables for the cooling light and the light is fed into other slaves on the experimental tables. For $^{85/87}$Rb the repump light, as already mentioned, does not have to be high power(4 mW is sufficient) and does not need to be amplified past the master table. Also the light frequency needs to be shifted to the appropriate frequencies using AOMs on the experimental tables.

4.5.2 Lithium

For Rb there are masters dedicated for each of the repump light and cooling light of both Rb 85 and Rb 87, there is only one master used for the lithium light. The lithium setup on the master table therefore has an added layer of complexity where the light from the slave that the master injects has to be used for both repump and cooling light. Fig.4.13 shows a simplified version of the Li setup on the master table explaining the frequency shifting of the master light and the slaves involved. Light from the Li master initially injects a slave to amplify the master light. The light from this slave is passed through a 'double pass' setup where the frequency of the light is shifted once by the AOM then reflected back through the AOM and reflected again giving a double frequency shift. Light from this first double pass is at the frequency used for the cooling light of Li and part of this light is used to inject the Li cooling slave on the master table. The rest of the light from the first double pass AOM is sent through another double pass AOM setup which brings the light to the frequency needed for the Li repump light. This light is injected into the Li repump slave.

Light from each slave is divided among three fibers, two for experimental purposes and one for the diagnostics. On the experimental tables there are

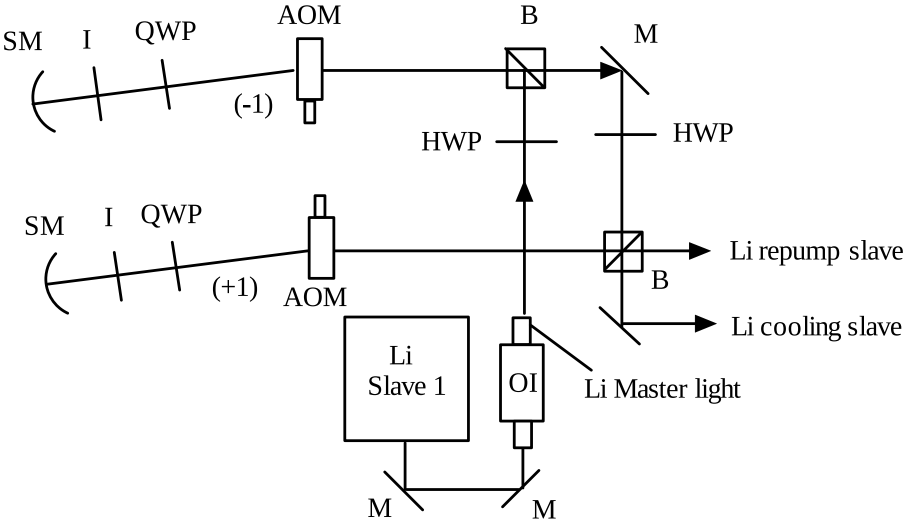

Figure 4.13: Lithium slave amplifier setup on the master table. A first slave (Li slave 1) is injected by the Li master. The light from this slave is intially reflected from a beamsplitting cube (B) and is sent through an acousto-optical modulator(AOM) and the (-1) order let through by an iris (I). A spherical mirror (SM) reflects the (-1) order back through the AOM such that the (-1) order again is selected going back. This means the beam frequency is now shifted downwards by 2 times the rf frequency sent to the AOM as compared to the original beam frequency. A quarter wave plate (QWP) is used so that the beam coming out of this double pass setup will pass through the beam splitting cube. Light from this first double pass is then split using a half wave plate (HWP) and cube(B) to send some of the light to inject a slave and the rest is sent to a second double pass setup where the light is further shifted and sent to inject a third slave. The frequency shifts chosen for the first and second double pass setups are such that the light injecting the second slave is at the correct frequency for laser cooling of ^{6}Li and the light injecting the third slave is at the frequency needed for repumping.

slaves for both the cooling and repump light which are injected from the light sent from the master table slaves. Unlike rubidium however no further frequency shifts are needed on the experimental tables. Ref. [Sin07] gives full details of the Li setup.

4.6 Problems and Fixes

This section provides an insider's view to some of the challenges experienced to get the masters and slaves operating at the level described above.

4.6.1 Frequency instability and locking issues

Acoustic resonances

When the saturated absorption optical setup was first set up and sent to the lock box to generate an error signal, upon zooming in to lock the error signal was so noisy there was not a well defined zero to lock to. It was noticed that people's voices made the signal vibrate even more and it was proposed that these were acoustic resonances in the springs and mounting equipment inside the ECDLs. To fix this the springs were stretched and sorbathane was placed in between the spring coils. To diagnose whether an improvement was made we subjected the masters to acoustic frequencies from a loud speaker, Ref. [Sin07] describes the experimental setup and data collection. The improvements made were noticeable in that the acoustic resonances were dampened and shifted to higher frequencies with the effect being that the noise on the error signal decreased to the point that we were able to lock the masters.

Feedback from slaves

When the slave injection is aligned very well, some of the slave light being rejected from the side port of the isolator will come straight back to the masters. Even with 40 dB attenuation from the isolators the amount coming back is sufficient to cause the master to be slightly unstable in frequency. The resulting error signal will have ripples making it harder to lock and reducing the stability of the master. This effect was sufficiently damaging for the Li Master that the Li MOT created on the photoassociation experimental table was visibly wobbling and not stable.

Different methods were used to try to reduce this effect. One method was that the injection to the slaves (and therefore the back reflection to the masters) was slightly misaligned which reduces the amount of slave light going back to the master. This had the disadvantage of narrowing the frequency range over which the slave could inject. A second method was to place neutral density (ND) filters in the path of the injection beam to cut down the amount of light going to the master, this also cut down the amount of injection power to the slaves which makes injection more difficult. The last and best solution was to put a second isolator in front of the masters to better isolate the masters from the slave light, this allowed the alignment to be optimal and the injection power not cut down. Also the lithium MOT on the photoassociation/Feshbach experimental table was visibly more stable once this solution had been implemented. The repump masters have isolators while the Rb cooling masters do not as their error signals were large enough to not be washed out by the ripples although it may be beneficial to install secondary isolators for these masters as well.

4.6.2 Li Slaves

Because the free running wavelength of the Li slaves is quite far from the frequency at which they are injected, getting the Li slaves to inject has presented some difficulty. Using the Booth factor technique described in section 4.4.3 we have been able to inject the slaves at lower temperatures, 68 degC, instead of the initial 78 degC at which we were injecting them. An improved injection alignment, therefore, allowed the slaves to be pulled farther in frequency from their free running frequency and widened the injection range. Once injected, if the injection frequency is not changed they are quite stable over several days. A problem arises however when the injection frequency is changed or the injection light is shuttered by turning on and off the shift AOM's. In these cases the injection would not necessarily follow or be reestablished.

For the Li slaves it was found that the current at which they are run affects their ability to follow injection changes, with a lower current giving higher stability, unfortunately this reduces the power available to be used for experimental purposes. Other factors that helped improve the injection response of the Li slaves were the alignment of the shift AOMs such that changes in the double pass efficiencies(the percentage of light power coming out of the double pass setup as compared to the amount sent in) for different frequencies to the AOM were minimized. Also the irises in the double passes if not placed properly will clip the beam passing through them when the AOM frequency is changed.

Temperature drifts

Once locked, the slave lasers maintained a constant frequency for several hours. Attention was called to the fact that the masters were not well isolated from temperature drifts external to the master housing though they are temperature controlled.

To isolate the master boxes further from the outside environment a plastic, foam insulated box was constructed surrounding the masters on all sides. In addition a fan and a heat conduit were installed to steadily remove the heat coming off from the Li heat pipe. Finally it was agreed to leave the curtains protecting the master table from dust and air currents up unless work on the master table necessitated their removal.

With these measures the locking time for the masters improved up to several days. The ^{85}Rb cooling master however despite these changes would not stay locked for more than a couple of hours, the resolution of this is described in the next subsection.

4.6.3 Untoward incidents

The following contains a description of some of the component failures that have been associated with master's not properly functioning, either not locking or not lasing stably at the desired frequencies.

Not so super glue

The piezo directly behind the grating is glued (using super glue) to an aluminum piece attached to the same mount on which the laser diode is secured (see Fig. 4.2). The grating is glued to the piezo. On several occurences (twice for the ^{85}Rb cooling master and once for the ^{87}Rb cooling master) either the grating or the piezo and the grating have started falling off the mount. This can be attributed to the surfaces to which the super glue was applied not being clean, being rough, or having too much glue applied. Also, the pieces may have been moved while the glue was drying, weakening the bond. Conversely the glue seems to work quite well when an object needs to be replaced or removed. In this case, acetone works well to dissolve the glue and continual soakings around the edges of the object with acetone and patience as well as razor blades (used with extreme caution) helps. Gratings can not be cleaned and should never be touched directly or have acetone put on them.

TEC's

On one occasion (in the ^{85}Rb repump master), perhaps due to excessive strain while tightening down the laser mount, one of the conductive rows in the TEC crumbled. Also the TEC's leads are very fragile and have been known in other instances to come off.

Piezos

Despite experienced members in our lab never having seen a piezo 'blow' before we have had this occur twice to date. This can be recognized by the resistance across the piezo going to a small resistance (several ohms) from its typical infinite resistance. The length piezo in the ^{85}Rb repump master failed, as did the angle piezo in the ^{85}Rb cooling master. Possible reasons are power surges during power outages or prolonged exposure to voltages > 150V. There is now a mix of piezos in the master laser housing from Piezomechanik, Thorlabs and Noliac. The piezos from the first two companies have a maximium voltage of 150V and the piezos from Noliac have a 200V limit. The piezo drivers used in the lab run up to 200V and could lead to the failure of the piezos. The failure of a piezo can be identified by the absorption signal from the saturated absorption lock not responding to changes in the settings for that piezo.

The leads of the piezos fall off very easily and do not resolder well, a resoldered lead to the piezo behind the grating was found to be the reason the ^{85}Rb cooling master was not locking for long periods of time, with replacement of the piezo this has been fixed. Another potential improvement for this master was the replacement of plastic screws attaching the grating and piezo mount to the laser diode mount with metal screws, perhaps reducing drift in the position of the grating.

Chapter 5

Miniature atom trap table - Dual injection study

The miniature atom trap table is one of the experimental tables that can be sent light from the master table. This table is dedicated for the purpose of the study of creating a more portable system for creating magneto-optical traps making this physics more accessible for educational purposes. Dr. Jim Booth from the British Columbia Insitute of Technology (BCIT) is directing this study in collaboration with our lab. The MAT table had the first operational ^{85}Rb or ^{87}Rb MOT working in our lab. Towards the end of making the setup for magneto-optical traps more compact a study was undertaken of the dual injection of a single Rb slave by both ^{85}Rb and ^{87}Rb cooling light to create a dual ^{85}Rb and ^{87}Rb MOT. This chapter will detail this experiment and the results obtained.[1]

5.1 Experimental setup

The experimental setup is shown in Fig.5.1. Injection light for subsequent amplification was generated by two Rb masters, M1 and M2, at frequencies ν_1 and ν_2. A variable fraction of light from each master was combined into the injection fiber FC1 by running the fiber splitters for the Rb setups on the master table backwards. Light from possibly two other masters, M3 and M4, was coupled into fiber FC2. Fig. 5.2 shows the details how the light from the master table was coupled into fibers FC1 and FC2.

The injected slave laser light and the light from FC2 were double passed to bring them to the frequencies needed for the intended usage of magneto-optical trapping. The characterization of the frequencies being output from the slave laser was achieved by overlapping the slave laser light and light

---

[1] A version of this chapter has been submitted for publication. Booth, J.L., Van Donen, J., Lebel, P., Klappauf, B.G., and Madison, K.W., Dual-channel amplification in a single-mode diode laser for multi-isotope laser cooling. J. Opt. Soc. Am. B/ Vol. 24, No. 11/ November 2007

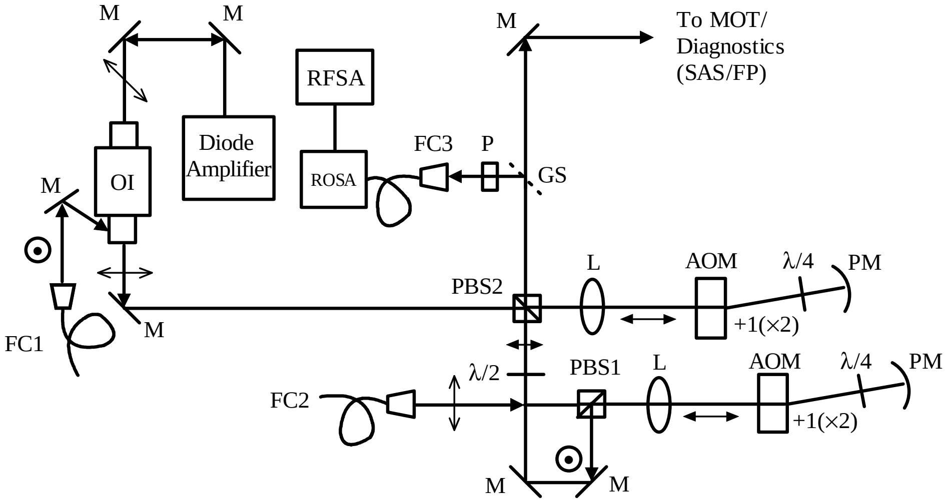

Figure 5.1: Vertically polarized light from fiber FC1 injects the slave diode amplifier. The light from both the amplifer and from FC2 is shifted in frequency in double pass setups and combined at a polarizing beam splitting cube (PBS2). Part of both beams is then sent by a glass slide (GS)to a photodector (ROSA) and the homodyne and heterodyne beam notes detected on a RF spectrum analyzer. The rest of the light power is sent to a saturated absorption spectrometer (SAS), a Fabry-Pérot, and the optics for a magneto-optical trap. Labelling: (M) mirror, (L) lenses, (AOM) acousto-optical modulator, ($\lambda/4$) quarter wave plate, (OI) optical isolator, (P) polarizer, (PM) parabolic mirror

from FC2. A small portion of this overlapped light was redirected by a glass slide (GS) and coupled into fiber FC3. Because the two beams have orthogonal polarization after combining on PBS2, a linear polarizer (P) was used to mix and purify the polarization before coupling them into FC3. The light coupled into FC3 was sent to a high speed photodetector(receiver optical subassembly (ROSA), Advanced Optical Components, 10Gbits/s, GaAs PIN photodiode and preamplifier) whose output was recorded on a rf spectrum analyzer[(RFSA), Agilent model E4407B]. A power of less than 100 μW exiting the fiber was used to detect the heterodyne and homodyne beat signals (heterodyne meaning beats arising between the slave light and the light from M3 and homodyne meaning the beats between the multiple frequencies out-

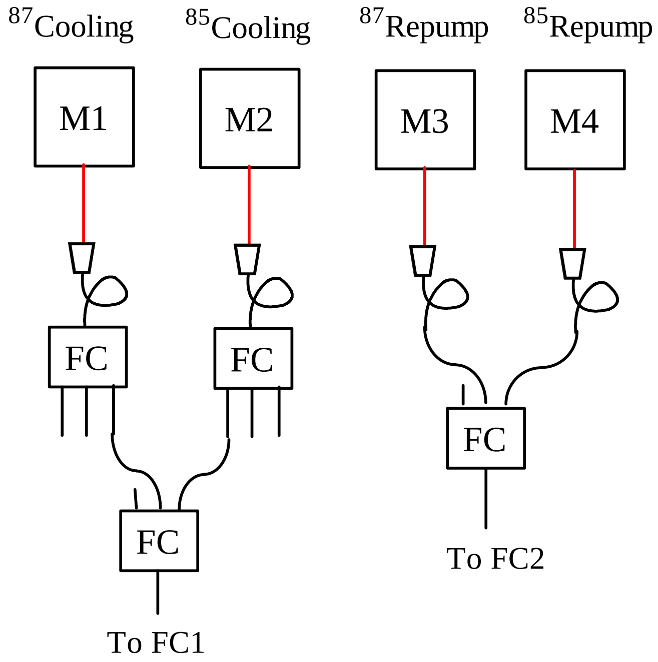

Figure 5.2: Fiber setup for dual injection experiment. Light from masters M1 and M2 (red lines indicate light) are coupled into fibers and combined in fiber combiners (FC) and sent to the MAT table by fiber FC1. Light from masters M3 and M4 are also coupled in fibers and combined and sent to the MAT table by fiber FC2. Above each master is written which particular master was used, though in this experiment the actual usage of the masters was not always what they were originally intended for in terms of laser cooling and trapping. The extra lines indicate extra fibers in the combiners that were not used.

put from the slave laser itself). Note that for the characterization studies only light from M3 outputting frequency ν_c(c for comparison) was sent to fiber FC3. The amplifer output was also characterized using a saturated absorption spectrometer (SAS) and a confocal, scanning Fabry-Perot (FP) interferometer with a free spectral range of 5.0 GHz and a linewidth of 25 MHz.

For these dual injection studies, the slave amplifier current and temperature were optimized for operation at the cooling transitions used in our lab for ^{85}Rb and ^{87}Rb (denoted $\nu_{3-4'}$ and $\nu_{2-3'}$) respectively. Using the FP and SAS diagnostics, we verified that at the optimal settings the slave laser diode would reliably amplify light from only one master as it scanned continuously over a range of approximately 1.5 GHz. The center frequency of this range was adjustable by changing the current of the amplifier.

Multichannel amplification(amplification of multiple frequencies) in semiconductor lasers has been studied extensively in the past, especially as it relates to optical communications [Agr95, TTNR99]. Two important phenomena associated with this technique are gain saturation and four wave mixing (FWM). In gain saturation, because the finite amplifier output power is shared among several frequencies, the gain and resulting output power of each frequency is limited by the power extracted by the other frequencies. FWM results from the strong coupling of the optical fields and electron carrier density(which determines the gain and refractive index) inside the gain medium. The injected fields can induce spatial and temporal modulations of the carrier density. These modulations in turn produce scattering of the fields present within the gain medium (nonlinear wave mixing) generating new frequency components. In particular, for a frequency difference between the two injection lasers of $\Delta = \nu_1 - \nu_2$, FWM fields will appear at frequencies

$$\nu_n^{(FWM)} = \nu_i + n\Delta \tag{5.1}$$

where $i = 1, 2$, and integer n, we will refer to as the FWM order.

The detection of heterodyne beat signals allowed characterization of the output spectrum with very high resolution (< 10 MHz), limited only by the resolution bandwith of the RFSA and by a convolution with the output spectrum of the comparator laser, M3, which had an emission linewidth of ~ 2.0 MHz. The rf beat note spectrum detected by the ROSA contained signals at the difference frequencies of all the harmonic components of the incident field, $|\nu_i - \nu_j|$ where $\nu_{i,j}$ is any frequency in the set containing $\nu_n^{(FWM)}$, ν_1, ν_2, and ν_c. In the absence of ν_c, the homodyne beat spectrum will be generated by pairs chosen from the set $\{\nu_n^{(FWM)}\}$ (which includes $\nu_{1,2}$) and will only contain rf frequencies $f_m^{(rf)} = m\Delta$, where $m = 1, 2, 3, \cdots, p-1$ and p is the total number of frequency components present in the amplifier optical spectrum. The number of pairs contributing to a given rf frequency component will be $q = p - m$. Therefore the total rf power at this frequency will result from a sum over the product of the field amplitudes $|E_i E_j^*|$ taking into account the different rf phases, which will result from differences in the optical phases of the contributing fields at the detector. Without knowledge of the optical phases, the optical spectrum cannot be reliably extracted from the homodyne spectrum. These ambiguities are removed through heterodyne detection with an independent comparator laser field at ν_c chosen such that the frequency differences $\nu_c - \nu_{1,2}$ are each incommensurate with Δ. In principle, both the phase and the amplitude of the components $\nu_n^{(FWM)}$ are accessible using this techinique. Expressing the comparator detuning as $\delta = \nu_1 - \nu_c$ and assuming that both δ and Δ are positive, distinct heterodyne beat notes will occur at

$$f_{+n}^{(rf)} = |\nu_c - \nu_{+n}^{(FWM)}| = \delta + n\Delta \tag{5.2}$$

for positive orders ($n > 0$) and

$$f_{-n}^{(rf)} = |\nu_c - \nu_{-n}^{(FWM)}| = |\Delta - \delta| + |n|\Delta \tag{5.3}$$

for negative orders ($n < 0$). The $n = 0$ terms yield the beat note frequencies between the seed and comparator fields.

5.2 Results

5.2.1 Dual Frequency Amplification

Fig.5.3 shows an RF heterodyne and FP spectrum of the amplifier output. For these data, the amplifier was injected with two fields at frequencies ν_1 and ν_2 each with 0.7 mW. M1 was locked 180 MHz to the red of the ^{87}Rb cooling transition ($\nu_{2-3'}$). M2 and M3 were locked at $\Delta = 73$ MHz and $\delta = 53$ MHz to the red of M1 respectively. The amplified seed frequencies at ν_1 and ν_2 contained more than 80% of the total optical power (50 mW at a diode current of 100 mA). The spectral width of the amplified seeds was the same (to within < 100 kHz) as that of the input seed beams, determined by the heterodyne beat note with M3.

We also observed that the relative output power at the two seed frequencies could be varied by changing the input seed powers. This control is

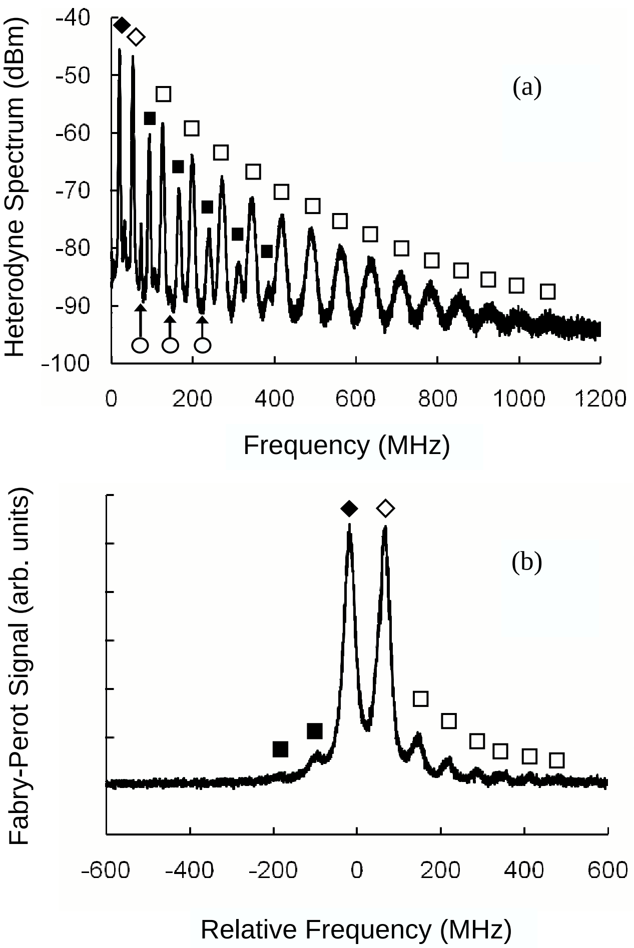

Figure 5.3: (a) RF heterodyne and (b) FP spectrum of the laser diode amplifier. The two seed beams were 0.7 mW each and $\Delta = 73$ MHz apart. After amplification more than 80% of the total optical power (50 mW at a diode current of 100 mA) was contained at the seed frequencies, ν_1 and ν_2, labeled by (◇) and (♦) respectively. The additional FWM components generated in the amplifier are labeled by (□) and (■) for the positive and negative orders respectively. The comparator frequency ν_c was chosen to be $\delta = 53$ MHz below ν_1 to provide a distinct heterodyne beat note for each of the FWM components. The amplifier homodyne beat notes are labeled by ($\circ$). For this heterodyne spectrum, the power incident on the ROSA from the amplified beam and from M3 was 11.5 μW and 12.0 μW respectively.

provided by gain saturation and was studied by fixing the amplifier current to 101.4 mA and the seed power from M1 at 0.67(3) mW and then varying the injected power from M2. A FP trace for each combination of input powers was recorded and the relative amplitudes of the peaks corresponding to frequencies, ν_1 and ν_2 were recorded. The data are shown in Fig.5.4. The output powers of the two seeds were observed to be equal when the power from M_2 was 0.8 mW. The power balance of the two seeds was also observed to depend on the amplifier current, providing another method to control the power ratio.

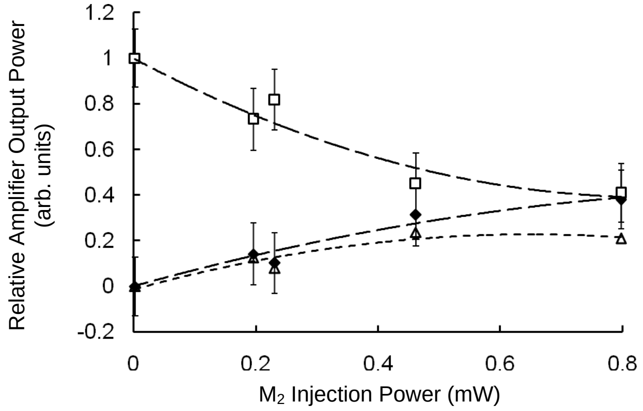

Figure 5.4: Relative amplifier power output in the two seed frequencies, ν_1 (□) and ν_2 (♦), as a function of the injected power at ν_2 from M2 with the input power from M1 held fixed at 0.67(3) mW. The sum of the power contained in the FWM components is also shown (△). At almost equal injection power, the amplified seeds were equal in amplitude and contained approximately 80% of the total output power. The dashed lines are a guide to the eye.

The amplifier output also contained both positive and negative FWM sidebands and these are clearly visible on the FP and heterodyne spectra. The heterodyne beat detection provides a much greater sensitivity (i.e. signal to noise) than does the FP and many more FWM orders are visible in this spectrum. The width of the FWM beat notes and therefore the corresponding optical linewidth increases with order number (see Fig. 5.5). To our knowledge, this behavior has not been reported in semiconductor laser amplifiers and this characteristic of the FWM orders is not evident from the

FP trace due to its limited resolution (25 MHz). Second, we observe that the amplitude of the high frequency FWM orders is larger than the low frequency orders. FWM gain asymmetries have been previously observed and it has been asserted that this is an inherent characteristic of semiconductor laser amplifiers.

The homodyne signals were also observed at integer multiples of Δ. As discussed earlier, the number of pairs contributing to a given RF frequency component at $f^{(rf)} = m\Delta$ in the homodyne signal is $q = p - m$, and the relatively low amplitude of these signals is probably due to phase differences of the RF contributions (originating from phase differences in the optical fields) which tend to cancel when summed if the phase differences exceed $2\pi/q$.

The heterodyne beat signals were each fit to a gaussian to yield the center frequency and full width half maximum (FWHM) and these are plotted as a function of FWM order in Fig.5.5. The FWHM, $\Delta f_n^{(rf)}$, of the RF components was observed to scale linearly with the order, n, and the positive order (higher frequency) FWM components follow $\Delta f_{+n}^{(rf)} = 3.05(10)\,|n| + 2.05(86)$ [MHz] in agreement with the linear fit to the negative order FWM data, $\Delta f_{-n}^{(rf)} = 3.01(17)\,|n| + 2.23(60)$ [MHz]. The same linear behavior of the FWM component widths with order number (but with slightly different slopes) was observed for each combination of injection frequencies for Δ ranging from 73 MHz up to 6.6 GHz.

5.2.2 Applications

In this section, we report three different experiments which were performed to demonstrate the applicability of dual-frequency amplification to laser cooling and trapping of atoms. For all three experiments, the MOT quadrupole magnetic field gradient was 14(1) G/cm in the axial direction, the cooling and repumping beams were split equally into three retro-reflected beams 1 cm in diameter, and the residual background vapor pressure as measured by the ion pump current was 1.4×10^{-9} Torr.

First, a ^{87}Rb MOT was created by simultaneously amplifying both the cooling and hyperfine repump light for this isotope. The challenge was that the two seed frequencies were separated by 6.572 GHz, well outside of the range over which the amplifier diode laser was capable of continuously following a single seed. Nevertheless, we observed that the amplifier produced adequate gain at both frequencies to realize a MOT. The amplifier was optimized to operate at the cooling frequency ($\nu_2 = \nu_{2-3'}$) and produced 31.6 mW from a seed input of 0.7 mW while producing 4.2 mW of repump

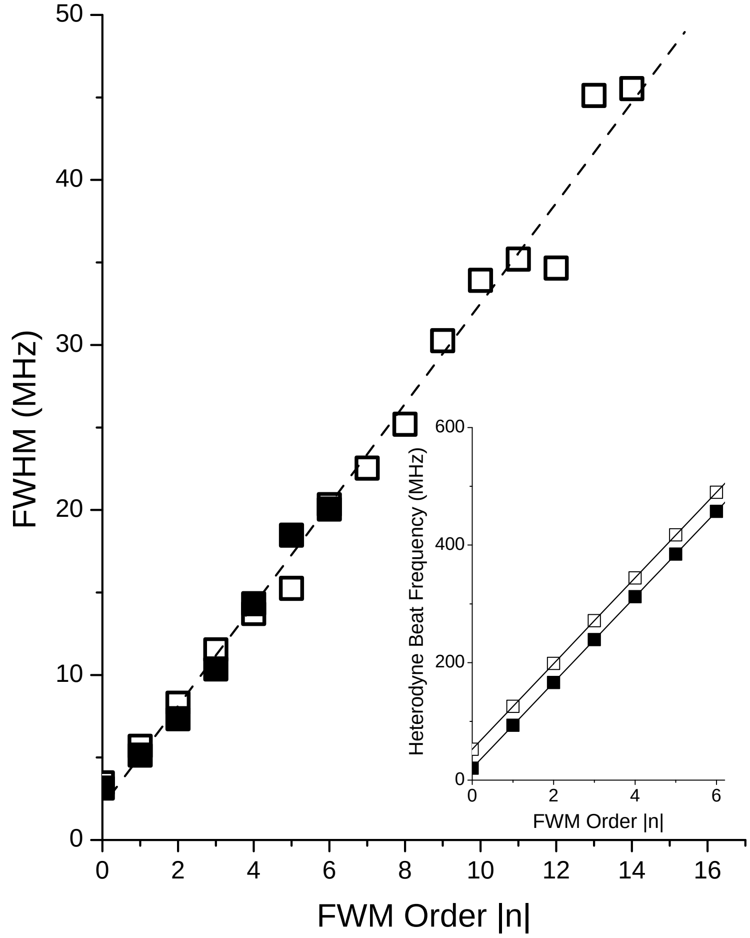

Figure 5.5: The heterodyne beat frequency width (FWHM) as a function of the FWM order for both positive and negative orders, labeled by (□) and (■) respectively. The inset shows the beat center frequency versus FWM order, and the slopes for the positive and negative orders provide a measure of $\Delta = 72.88$ and 72.85 [MHz] respectively. These data were extracted from the heterodyne spectrum shown in Fig.5.3.

light with a seed of 0.7 mW. Only the $n = -1$ FWM sideband (the one closest to the dominant ν_2 seed) was observable and contained <4.0 mW. In related work [MKP+96], Moon *et. al.*reported that an amplifier can be partially injected so that amplification is achieved while some light is still produced at the free lasing wavelength. By temperature and current tuning of the free lasing wavelength to the repump transition (6.8 GHz away from the injected seed), a Rb MOT could be formed using the two frequencies produced by the amplifier. In the second experiment, we wished to illustrate the importance and influence of the FWM optical sidebands generated in the amplifier. Not only do the FWM sidebands reduce the power available for seed amplification, they can also complicate spectroscopy and laser cooling by exciting additional transitions. In particular, for a rubidium MOT, only a few mW of power is needed for hyperfine repumping and such power was available in the FWM sidebands. A ^{85}Rb MOT was therefore created by amplifying the first seed tuned 2.7Γ ($\Gamma = 2\pi \times 5.9$ MHz) to the red of the cycling transition $\nu_1 = \nu_{3-4'}$ and by choosing ν_2 below ν_1 by $\Delta = 1.453$ GHz so that the $n = +2$ FWM sideband was resonant with the lower ($F = 2 \rightarrow F' = 2$) repump transition. The power produced was 23 mW, 12 mW, 5 mW, and 3 mW at ν_1, at ν_2, at the $n = +1$ FWM sideband, and at the $n = +2$ FWM sideband tuned to the repump frequency.

Perhaps the most important application studied was the creation of a dual isotope Rb MOT. Two seeds tuned 2.7Γ to the red of the two isotope cooling transition frequencies ($\nu_{2-3'}$ and $\nu_{3-4'}$) were simultaneously amplified. Two separate frequency stabilized master lasers, M3 and M4, provided a total of 8 mW of hyperfine repumping light for the two isotopes. These repump beams were combined in a fiber coupler and introduced to the experiment through fiber FC2 without amplification and collinear with the amplified light.

Data on the dual isotope rubidium MOT was acquired using a CMOS camera (Pixelink PL-A741) and by imaging the fluorescence onto a photomultiplier (EMI 9558B). To increase the fluorescence measurement signal to noise, we employed a lock-in amplifier (SRS SR830 DSP Lock-In Amplifier) and frequency modulated the amplified beam by ± 4 MHz at a rate of 5.00 kHz. The composition of the dual species MOT was controlled by interrupting the two hyperfine repump beams (approximately 4 mW from each was incident on the MOT) before the fiber coupler to alternately trap ^{87}Rb, ^{85}Rb, or both species. It should be noted that this manipulation was performed without altering the diode laser injection. For the dual MOT experiment, 80% of the total amplifier power (50 mW) was contained in the two seed frequencies which had equal amplified powers. Only five significant (less than 45 dB below the seed components) FWM components were detected in the output spectrum - four higher and one lower than the seed frequencies.

Fig.5.6 shows the MOT fluorescence signal for the dual isotope MOT as a function of time under various loading conditions. The MOT fluorescence curves were fit to an exponential to extract the loading rate as well as the equilibrium fluorescence levels of the single species MOTs. The filling time of the ^{87}Rb MOT was found to be 1.9(2) s compared to 0.7(1) s for ^{85}Rb - the more abundant isotope. The ratio of the filling rates 2.7(5) is consistent with the isotopic abundance of the two species (72.17% : 27.84% or 2.59:1). Whereas the equilibrium fluorescence levels (normalized to the dual MOT equilibrium value) for each single isotope MOT were 0.781(72) for ^{85}Rb and 0.396(94) for ^{87}Rb, and this ratio, 1.98(25), is not in good agreement with the isotopic abundance. This is most probably the result of the different light assisted collisional loss rates of each isotope in the MOT [WDT$^+$92].

The filling time of the dual species MOT was 0.7 s and its equilibrium fluorescence level was 15% lower than the sum of the single species MOT fluorescence providing evidence for collisional losses between the two species. In addition, under these experimental conditions the fluorescence of the ^{87}Rb recovered when the ^{85}Rb repump light was blocked, demonstrating that the equilibrium number of ^{87}Rb atoms in the MOT is reduced in the presence of a ^{85}Rb MOT (See Fig. 5.6). A similar recovery was not observed for the ^{85}Rb MOT, indicating that for these parameters the ^{87}Rb was the more weakly trapped isotope. Such observations have previously been used to quantify the inter-species light assisted collisional losses in a dual isotope Rb MOT [SWS$^+$94].

Fluorescence images were taken of the MOTs and are displayed in Fig.5.7. We observed that the two isotope clouds were well overlapped and superimposed with the location of the single species MOTs. The center positions were unchanged to within ±10 μ m when we switched from dual to single species mode. This observation demonstrates one of the primary advantages of this dual amplification approach to trapping multiple isotopes. Because the primary trapping frequencies emerge from the single mode amplifier in exactly the same spatial mode and polarization state and traverse exactly the same optical path (thus accumulating precisely the same aberrations and imperfections), the resulting positions and density profiles of the two MOTs are almost identical (the repump scattering rate in Rb for these MOT parameters is small enough that the radiation pressure from the repump light is a negligible perturbation to the trapping force).

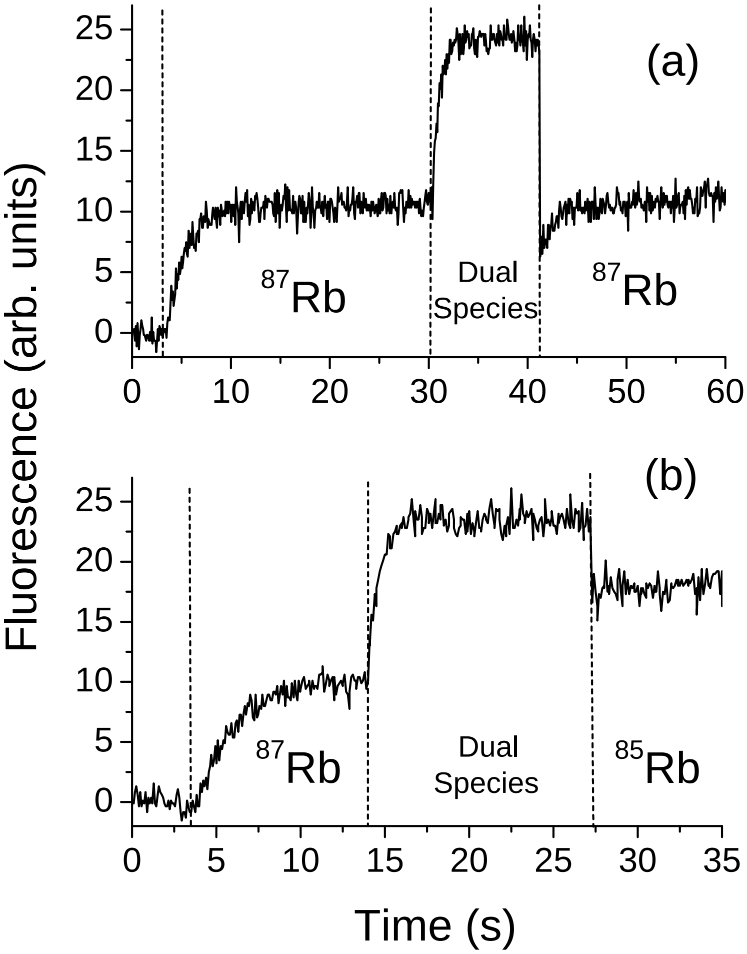

Figure 5.6: Fluorescence observed from the dual isotope rubidium MOT. The isotope loading was controlled by independently blocking the output of either the ^{85}Rb or ^{87}Rb repumping laser (M3 or M4) – which left the amplifier output unchanged. (a) The ^{87}Rb MOT was loaded by introducing its repumping light, and then the ^{85}Rb repumping light was introduced after 30 s. After the dual isotope MOT fluorescence reached steady state, the ^{85}Rb repumping light was extinguished. Immediately after, the ^{87}Rb fluorescence (proportional to the number of atoms) was observed to be lower than its steady state value in the absence of a ^{85}Rb MOT. After 3 s, the ^{87}Rb fluorescence recovered to its steady state value. In (b) after loading both isotopes, the ^{87}Rb repumping light was extinguished and the ^{85}Rb fluorescence level was observed to be unchanged by the presence of the ^{87}Rb MOT.

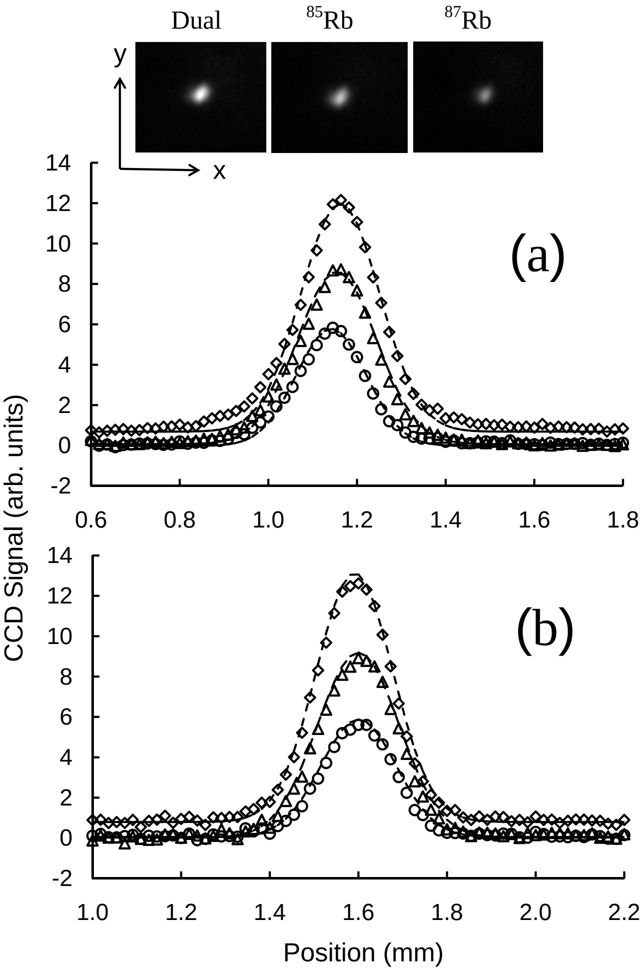

Figure 5.7: Images and line profiles of the atomic fluorescence from a ^{87}Rb (○), ^{85}Rb (△), and dual species (◇) MOT. The (a) x-axis and (b) y-axis center of mass of the single species MOTs was the same as the dual species MOT to within ±10 μm (±0.5 pixels where the magnification was 18 μm / pixel). The FWHM of the atomic cloud grew from a size of 220 μm for the single ^{87}Rb MOT to a size of 260 μm for the dual species MOT. We estimate that the atom numbers were 2×10^5, 1×10^5 for the single isotope ^{85}Rb and ^{87}Rb MOTs, and 2.6×10^5 for the dual isotope MOT.

5.3 Conclusions

We have investigated dual seed amplification in a single mode diode laser, have characterized the optical spectrum including the FWM sidebands in the highly degenerate regime, and have demonstrated that the output spectrum of the seeds as well as the FWM sidebands are appropriate for use in high resolution spectroscopy and laser cooling applications. In particular, we have used this amplifier to achieve simultaneous cooling and confinement of two isotopes of Rubidium (^{85}Rb and ^{87}Rb). One of the main advantages of this approach to trapping multiple isotopes is the fact that the primary trapping frequencies arrive at the MOT in the same spatial mode and polarization state resulting in almost the same trapping potential for the two isotopes. This feature alleviates the problems associated with imperfect mode matching and alignment of the two different trapping beams. We have also shown that the output power ratio at the two seed frequencies can be controlled using gain saturation in the amplifier. We reiterate that these results were achieved using an unmodified commercial diode laser with no additional AR optical coating applied. We therefore expect that similar results could be obtained with other diodes centered at different wavelengths. Improved performance over a wider bandwidth may be achieved when using AR coated diodes.

Chapter 6

Photoassociation and Feshbach resonance experiment

6.1 Experimental aim and outline

6.1.1 Feshbach resonance study

The aim of this study is to locate the magnetic field values at which Feshbach resonances occur between Li and Rb. By tuning the magnetic field the energy of two free atoms can be made degenerate with a molecular bound state so that the atomic pair, upon collisional relaxation, can be trapped in a molecular bound state [DVMR04]. The molecules initially formed are weakly bound [DFKMS04] and collisional relaxation refers to the collision of the atomic pair with a third particle (either another atom or a molecule) resulting in the weakly bound pair relaxing to a molecular bound state. To locate the Feshbach resonances we will load the atoms into an optical dipole trap (from a MOT) and sweep the magnetic field searching for values at which the number of atoms detected in the trap diminishes. The decrease is attributed to molecular formation.

The next experimental aim is the study of the application of Feshbach resonances to sympathetic cooling of Li with Rb. A standard MOT temperature of Rb is about 100 times colder than that of Li (tens of μK compared to 1 mK). Feshbach resonances allow the continuous tuning of collisional interactions and large scattering cross sections can be achieved providing a means of rapid thermalisation between Li and Rb. In this investigation Li and Rb will be precooled in a MOT and then loaded into an off-resonance optical tweezer. The magnetic field will then be swept through a Feshbach resonance to thermalise the ensemble. The Rb will again be laser cooled and the process repeated until the Li samples attain the same temperature as the Rb atomic cloud. The final stage of cooling will consist of evaporative cooling by slowly reducing the intensity of the optical tweezer beam.

6.1.2 Photoassociation study

The study the formation of heteronuclear LiRb molecules using photoassociation is another primary aim of the QDG laboratory and shares the same experimental table and apparatus as the Feshbach resonance study.

Fig.6.1 shows the principle of phooassociation of an atomic pair to a bound molecular state.

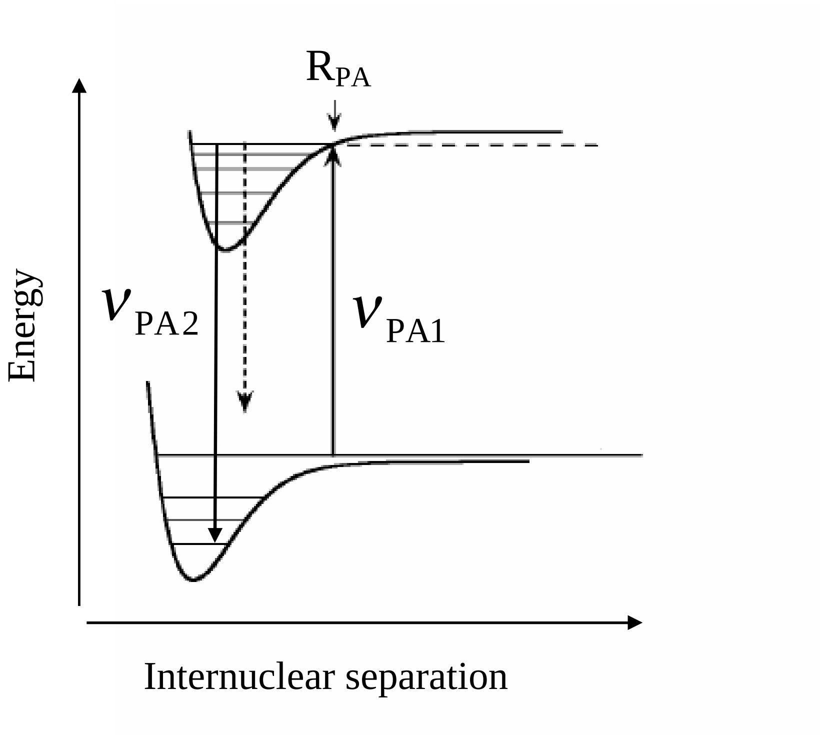

Figure 6.1: When the internuclear separation is less than R_{PA} unbound atoms can be brought by light of frequency ν_{PA1} to a molecular bound state. The atoms can decay (dashed line) to unbound atoms (as shown) or to a molecular bound state. The presence of light of frequency ν_{PA2} drives the population by stimulated emission to a ground electronic molecular bound state.

A colliding atomic pair in a free unbound state with internuclear separation less than R_{PA} can be brought to an excited molecular bound state energy with laser light ν_{PA1} tuned to that transition. The pair can then decay (dashed arrow) to a free unbound state or to a ground electronic bound state. The second option is favoured by introducing a second laser, ν_{PA2}

which causes the stimulated emission of the excited molecular state driving a transition to a ground electronic bound state.

Our initial experimental aim for this study is to characterize the rovibrational levels of the ground and excited molecular states. Again, losses in the number of trapped atoms will serve as an indicator of molecular formation. The frequencies, ν_{PA1}, at which losses occur will be mapped out and will provide information on the excited molecular bound states. In the presence of ν_{PA2}, transitions between the ground and electronic molecular states are AC Stark shifted. This means that the frequency at which ν_{PA1} causes losses due to a transition from the free atomic state to a particular excited molecular bound state is shifted to lower frequencies when ν_{PA2} is blue detuned from a transition of that excited molecular bound state to a molecular ground state. Conversely the ν_{PA1} resonance will be shifted to a higher frequency when ν_{PA2} is red detuned. When the frequency of ν_{PA2} is such that the resonance of ν_{PA1} is not shifted at all then ν_{PA2} corresponds to the proper separation of the excited molecular bound state from a particular ground molecular bound state. In this manner the ground molecular bound states can be determined by measuring the frequencies of ν_{PA2} at which the resonance frequency of ν_{PA1} is not shifted.

Having mapped out the molecular states, we will then attempt to make ensembles of moelcules in particular ground electronic states. Once the molecules are formed, the time evolution of the population of the initial quantum state can be monitiored using light at ν_{PA2} to re-excite the molecules back to the electronically excited state from where they can be photo ionized and the molecular ions can be detected using a time of flight (TOF) mass spectrometer. The mass selectivity of this spectrometer will help in discriminating the type of molecular ions formed.

6.2 Experimental Developments

The initial physical set up of the PA/Feshbach table is well described in Refs. [Sch07] and [Rau07] and will not be further reiterated in detail. Developments since the initial success of creating a dual species MOT consists of work on overlapping the Rb/Li MOTs, increasing the Li atom number in the Li MOT, compensation coil setup, stable injection of the Li slaves and finally the setup and testing of the optical dipole trap.

6.2.1 PA table light - brief summary

The experimental table used for the preliminary study of photoassociation and Fesbach resonances resides in Dr. David Jones's Lab and it is there that we have setup the capabilities of simultaneously cooling and trapping $^{85/87}$Rb and ^{6}Li atoms.

Either ^{85}Rb or ^{87}Rb repump and cooling light can be sent to the PA table from the master table. The $^{85/87}$Rb cooling light sent from the master table injects a slave on the PA table and the output of that slave is shifted by an AOM to bring it to the appropriate frequency for laser cooling. The AOM causes a loss of power in light so the light after the AOM is sent to another slave which at last is the light sent to the optics for the MOT.

Repump light from the master table for ^{85}Rb or ^{87}Rb is sent by fiber and shifted in frequency by another AOM and is sent to the MOT optics.

There are two lithium slaves on the PA table that are injected by the cooling and repump light from the master table, as discussed no further frequency shifting is needed. Light from all the slaves on the PA/Feshbach table is sent to fibers which are sent to the diagnostics on the master table.

6.2.2 Spatial overlap of the dual MOT

Because of power imbalances in the beams and imperfect alignment of the lithium MOT beams with respect to the rubidium beams when a dual Li/Rb MOT was achieved the Li and Rb MOTs were spatially separated instead of overlapping. Spatial overlap is important as we would like to perform experiments involving the interaction of the two species. To help overlap the two MOTs it has been useful to start with aligning the RB MOT (since the Rb beams are smaller) to markers on the magnetic coils (see Fig.6.2 showing part of the experimental setup) and then fine tuning the alignment such that the atomic cloud trapped in the Rb MOT expands uniformly from the center of the magnetic field. The larger Li beams can then be aligned with separate mirrors to the same markers on the coils with final adjustment to alignment and relative power of the beams in three different axis until the two MOTs are overlapped from different perspectives viewing with several cameras. Difficulties arise since the Rb and Li beams share the same optics in the MOT so that it is difficult to optimize both MOTs simultaneously.

6.2.3 Increasing the Li atom number

Because the Li slaves needed to be heated to temperatures close to their maximum temperature the power output of the Li slaves was substantially

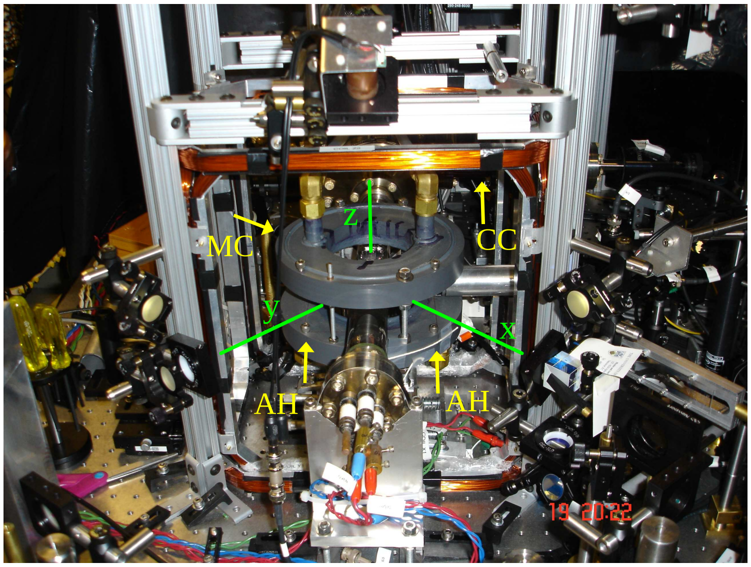

Figure 6.2: The magneto-optical trap setup on the photoassociation/Feshbach experimental table. The green lines indicated the axes along which the beams forming the MOT travel. The beams are aligned to alignment holes (AH) in the housing containing the magnetic coils (MC) that provide the magnetic field for the MOT and for the study of Feshbach resonances. Compensation coils (CC) help to center the MOT to compensate for power mismatches in the counterpropagating beams that displaces the atoms from the center of the MOT.

smaller compared to lower temperature operation (28 mW at 68 °C vs 56 mW at 23 °C for a current of 148 mA).

For this reason the set up of the MOT optics was altered to be a retroreflection MOT. In this configuration instead of splitting the incoming beams to generate one pair of cooling beams traveling in opposite directions, the beam is simply sent back by a mirror. This has the effect of doubling the intensity and we were able to obtain $\sim 2 \times 10^7$ Li atoms in the MOT. This may also help to spatially overlap the beams since the beams no longer are split(passing through a half wave plate and beamsplitting cube) simplifying the alignment of the beams. One immediate effect of changing to the retroreflection setup for the MOT optics was that because of the losses at each interface of the cell, the retroreflected MOT beams have lower power than the incoming MOT beams. This imbalance results in a displacement of the MOT from the center of the magnetic field.

Table 6.1 shows the detunings of the cooling and repump beams at which maximum fluorescence of the Li atoms was attained for varying currents sent through the magnetic coils used for the MOT.

I_{coil} (A)	δ_c (MHz)	δ_r (MHz)
3	-34	-20
4	-34	-24
5	-38	-20

Table 6.1: Detunings of the cooling and repump beams, δ_c and δ_r respectively, giving maximium Li fluorescence for different currents I_{coil} sent through the magnetic coils.

6.2.4 Compensation coils

In each of the directions of the MOT beams there are a pair of coils outside the MOT structure that are in a Helmholtz configuration and can be used to apply a magnetic field on the trapped atoms perpendicular to the plane containing each pair of coils. The compensation coils can then be used to move and center the atoms trapped in the MOT.

The compensation coils initially were not functional because the metal housing used to constrain the compensation coils was not electrically isolated from the coil wires due to metal screws used to fasten the coils and possible contact between the wire and the coils at the stress points near the bends of the coil housing. Electrically isolating the compensation coil housing from the frame to which they mount by covering the metal screws with heatshrink tubing and using plastic washers and screws worked to make the compensation coils operational.

6.2.5 Optical dipole trap

The trap laser is a 20 W, 1064.3 nm fiber laser from IPG Photonics (Model: YLR-20-1064-LP-SF). The initial stage of the trap development is first to try a single pass trap where the laser is strongly focused and the atoms are trapped at the focus. The next is to retroreflect the beam back creating a standing wave trap increasing the intensity and to measure the improvement in trapping. The final version of the optical dipole trap is planned to be a resonator cavity. Fig.6.3 shows the trap setup to be implemented, this setup is predicted to give a focus of $\sim 50\mu$m at the center of the cell if lenses L1 and L2 are 185 cm apart and L2 is 41.5 cm from the center of the MOT.

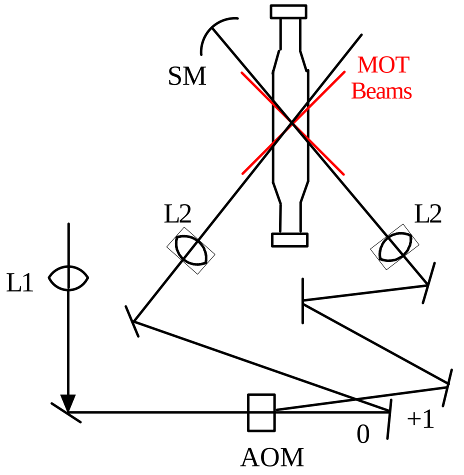

Figure 6.3: Schematic of the optical dipole trap setup. Light from the fiber laser is sent through an AOM and either the (0) or (+1) order used for trapping. As shown the (+1) order would be used as a standing wave trap and the (0) order would be a single focused beam trap. The lenses L1 and L2 are placed so that the beam is focused at the AOM and at the center of the MOT. The trap beams should be aligned to be at brewster's angle to reduce power losses.

An AOM from an old antares laser will be used to switch off the light when needed with either the zero or first order beam being used. Potentially the first order beam can be used as a standing wave trap to initially collect the atoms and the zero order could be used for evaporative cooling. The AOM gives a typical efficiency in the first order of 76 percent, however unfortunately this AOM is not AR coated for 1064 nm light so that we have $\sim$ 15 percent losses. This means that of the 20W from the fiber laser only a measured power of $\sim$ 11 W goes into the first order.

The current state of the work on the optical dipole trap is the alignment of the trap so that the focus intersects the MOT.

Bibliography

[Agr95] G. P. Agrawal. *Semiconductor Lasaers: Past, Present and Future.* AIP Series in Theoretical and Applied Optics, 1995.

[AWB98] A. S. Arnold, J. S. Wilson, and M. G. Boshier. A simple extended-cavity diode laser. Rev. Sci. Inst. **69**, 1236, 1998.

[CTDRG92] C. Cohen-Tannoudji, J. Dupont-Roc, and G. Grynberg. *Atom-Photon Interactions.* John Wiley and Sons, Inc., New York, 1992.

[DFKMS04] J. Doyle, B. Friedrich, R.V. Krems, and F. Masnou-Seeuws. Quo vadis, cold molecules? Eur. Phys. J. D. **31**, 149-164, 2004.

[Dra96] G. W. F. Drake. *Atomic, Molecular, and Optical Physics Handbook.* AIP Press, New York, 1996.

[DVMR04] S. Dürr, T. Volz, A. Marte, and G. Rempe. Observation of molecules produced from a bose-einstein condensate. Phys. Rev. Lett, **92**, 020406, 2004.

[Gri89] D. J. Griffiths. *Introduction to Electrodynamics.* Prentice-Hall, Inc., New Jersey, 2 edition, 1989.

[GWO00] R. Grimm, M. Weidemüller, and Y. B. Ovchinnikov. Optical dipole traps for neutral atoms. Advances in Atomic, Molecular and Optical Physics, vol. 42, p. 95-170, 2000.

[Had86] G. R. Hadley. Injection locknig of diode lasers. J. Quantum Electronics, **22**, no. 3, 1986.

[HJICDL02] W. Hofstetter, P. Zoller J. I. Cirac, E. Demler, and M. D. Lukin. High-temperature superfluidity of fermionic atoms in optical lattices. Phys. Rev. Lett. **89** 220407, 2002.

[HWS01] C. J. Hawthorn, K.P. Weber, and R. E. Scholten. Littrow configuration tunable external cavity diode laser with fixed direction output beam. Rev. Sci. Inst. **72**, 4477, 2001.

[Joc04] S. Jochim. Bose-einstein condensation of molecules. Ph.D. Dissertation, Institut für Experimentalphysik, 2004.

[JTLJ06] K. M. Jones, E. Tiesinga, P. D. Lett, and P. S. Julienne. Ultracold photoassociation spectroscopy: Long-range molecules and atomic scattering. Rev. Mod. Phys., **78**, 2006.

[KE05] A. Keshet and P. Eugster. Unbelievable: The story of a laser. Internal report, 2005.

[KGJ06] T. Köhler, K. Góral, and P. S. Julienne. Production of cold molecules via magnetically tunable feshbach resonances. Rev. Mod. Phys., **78**, 2006.

[KMS$^+$05] M. Köhl, H. Moritz, T. Stöferle, K. Günter, and T. Esslinger. Fermionic atoms in a three dimensional optical lattice: Observing fermi surfaces,dynamics and interactions. Phys. Rev. Lett. **94**, 080403, 2005.

[ME88] P. W. Milonni and J. H. Eberly. *Lasers.* John Wiley and Sons, New York, 1988.

[MKP$^+$96] H. S. Moon, J. B. Kim, J. D. Park, B. K. Kwon, H. Cho, and H. S. Lee. Magneto-optic trap of rubidium atoms with an injection-seeded laser that operates at two frequencies. Appl. Opt., **35**, 5402-5405, 1996.

[Mv99] H. J. Metcalf and P. van der Straten. *Laser Cooling and Trapping.* Springer-Verlag, New York, 1999.

[Rau07] N. Rauhut. Towards ultracold lirb molecules. Diploma Thesis, 2007.

[Sch07] B. Schuster. Ultra-cold li and rb atoms in a magneto-optical trap. Diploma Thesis, 2007.

[Sin07] S. Singh. Progress towards ultra-cold ensembles of rubidium and lithium. M.Sc. Thesis, University of British Columbia, 2007.

[ST91] B. A. E. Saleh and M. C. Teich. *Fundamentals of Photonics.* John Wiley and Sons, Inc., New York, 1991.

[Ste98a] D. A. Steck. The angular distribution of resonance fluorescence from a zeeman-degenerate atom: Formalism. Internal Publication, 1998.

[Ste98b] D. A. Steck. Atomic motion in a standing wave of far-detuned light. Internal Publication, 1998.

[Ste01] D. A. Steck. Quantum chaos, transport and decoherence in atom optics. Ph.D. Thesis, University of Texas at Austin, 2001.

[SWS$^+$94] W. Süptitz, G. Wokurka, F. Strauch, P. Kohns, and W. Ertmer. Simultaneous cooling and trapping of ^{85}rb and ^{87}rb in a magneto-optical trap. Opt. Let., **19**, 1571-1573, 1994.

[Tas98] H. Tasaki. From nagaoka's ferromagnetism to flat-band ferromagnetism and beyond: An introduction to ferromagnetism in the hubbard model. arXiv: cond-mat/9712219, 1998.

[TT95] R. J. Knize T. Takekoshi, J. R. Yeh. Quasi-electrostatic trap for neutral atoms. Optics Communications, vol. 114, p. 421-424, 1995.

[TTNR99] J. Troger, L. Thévanez, P. A. Nicati, and P. A. Robert. Theory and experiment of a single-mode diode laser subject to external light from several lasers. J. Lightwave Technol., **84**, p. 629-636, 1999.

[WDT$^+$92] C. D. Wallace, T.P. Dinneen, K. Y. N. Tan, T. T. Grove, and P. L. Gould. Isotopic differenc in trap loss collisions of laser cooled rubidium atoms. Phys. Rev. Lett., **69**, 897-900, 1992.

[WH03] J. Weiner and P.-T. Ho. *Light-Matter Interaction*, volume 1. John Wiley and Sons, Inc., New Jersey, 2003.

[WPGH05] F. Werner, O. Parcollet, A. Georges, and S.R. Hassan. Interaction-induced adiabatic cooling and antiferromagnetism of cold fermions in optical lattices. Phys. Rev. Lett. **95**, 056401, 2005.

[Zar88] R. N. Zare. *Angular Momentum.* John Wiley and Sons, New York, 1988.